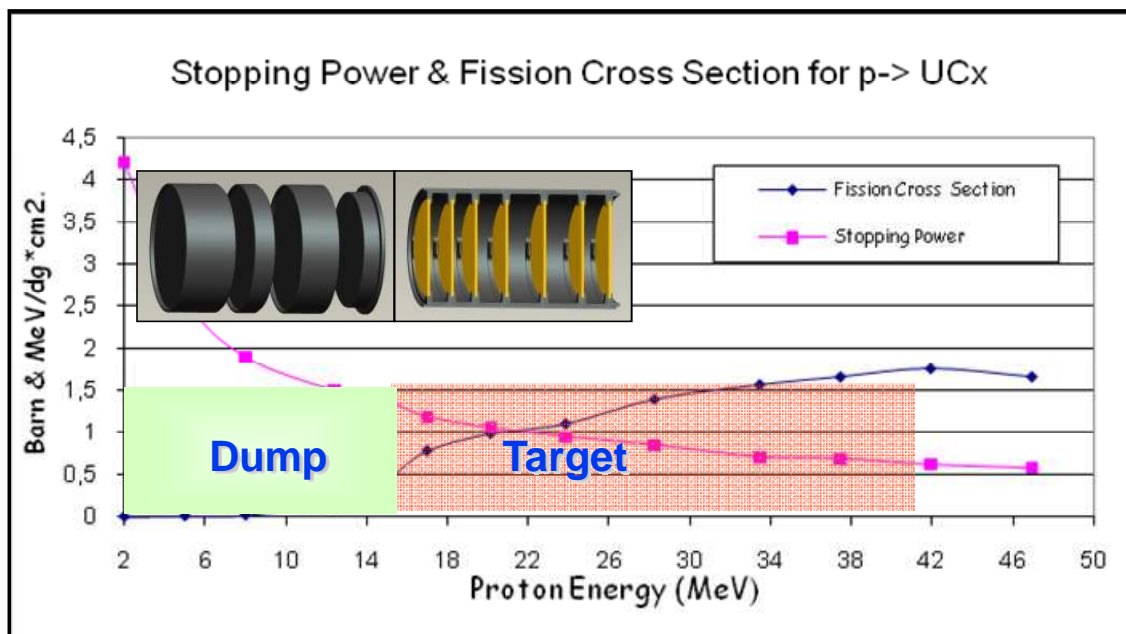


## THE PRODUCTION TARGET

### 5.1 The target concept

Three important parameters are required to optimize a fission ISOL target: first of all a high number of fission reactions (to provide high RIB intensities), then a low power deposition in the target materials (to avoid melting temperatures) and finally a fast isotope release time (to improve extraction efficiency). The main problem for a direct target configuration concerns the power deposited by the incident beam in the production target, mainly due to the electromagnetic interactions. In the SPES target this issue was addressed: only protons with energy high enough to have good  $^{238}\text{U}$  fission cross-section interact with UCx, the final part of the range is spent inside a graphite dump; the whole target was properly optimised from the thermal point of view.

As a matter of fact, the  $^{238}\text{U}$  fission cross-section and the stopping power have opposite dependency on the proton energy, as shown in figure 5.1 [1-4]. The low energy protons have high stopping power and release a high power in the target but are not so efficient for isotope production because their low fission cross-section.



*Figure 5.1: Stopping power and fission cross-section for protons on UC<sub>x</sub>.*

If the low energy protons (for example with energy lower than about 20 MeV) are driven towards a passive dump, the power deposited in the UCx target is lowered considerably and at the same time the number of fission reactions is maintained high. Moreover, the  $^{238}\text{U}$  fission cross-section increases with the proton energy up to 40 MeV and then stay constant. For energies exceeding 100 MeV, spallation enters in competition with the fission cross section and transuranium (alpha emitters) elements are produced complicating the radiation protection issue of the target management. With this in mind the target was designed for proton energy of 40 MeV and a possible upgrade up to 70 MeV will be considered in the future.

In order to optimize the heat dissipation and the release time of the fission products [5], a multiple disks target was proposed [6]: the target is split into several thin disks opportunely

spaced in the axial direction in order to improve the cooling of the  $UC_x$  target by thermal radiation and to avoid big temperature differences respect to the graphite box containing it. The advantage of this configuration is the simplicity of the cooling system and the consequent relatively low cost (see figure 5.2). The main characteristics of the SPES target are listed in the following [7]:

- the reference diameter of the target disks is 4 cm.
- the incident 40 MeV proton beam has a current of 0.2 mA. The beam profile spans uniformly over a circle distribution, which matches the disk radii;
- the window, necessary to separate the beam line from the target void regions, is made of one (or two) thin carbon foil of 400  $\mu\text{m}$  total thickness;
- the  $UC_x$  target (about  $\rho=3 \text{ g/cm}^3$ ) is made of seven disks about 1.3 mm thick each;
- the beam dump is made of three carbon disks about 0.9 mm thick each;
- the box containing the disks is made of graphite.

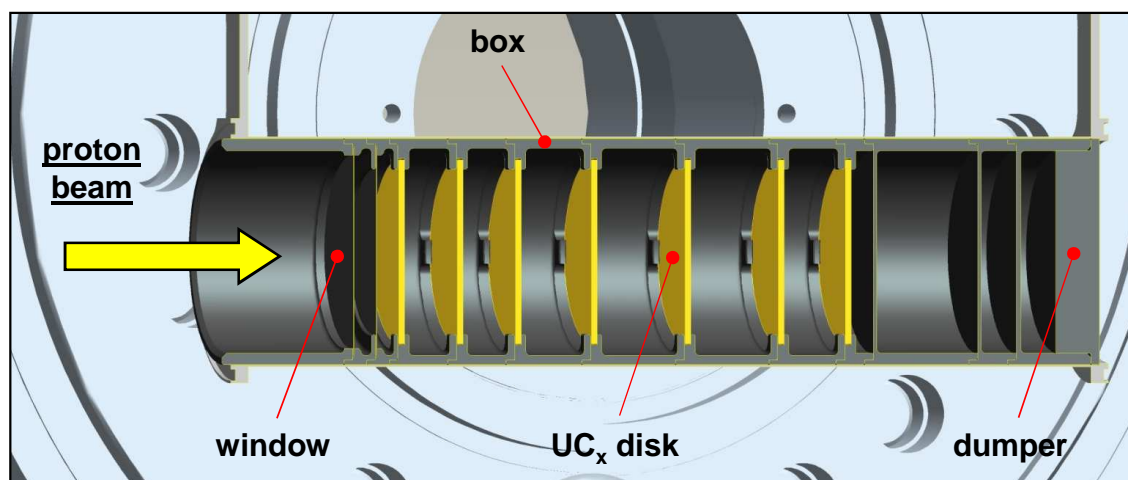


*Figure 5.2: Reference target configuration (the 7  $UC_x$  disks are shown in yellow).*

At this point it is important to observe that to guarantee an efficient RIB production rate the SPES target has to work at very high temperature levels, close to  $2000^\circ\text{C}$ ; the aforementioned proton beam power is not sufficient to heat the graphite box (containing the disks) up to the required temperature level because of the intense radiative heat exchange from the graphite box to the water-cooled chamber. As a consequence, it was crucial to introduce an additional and independent heating and screening system. It is important to underline that such heating device is completely independent from the proton beam and, additionally, allows for a better thermal control of the target when the proton beam power is not stabilized, i.e. during the start-up and the shut-down procedures. The target heating system consists of a thin tantalum (Ta) tube, with an average length of 200 mm, an external diameter and a thickness of 50 and 0.2 mm, respectively. It is welded at its edges to two tantalum wings, which are directly connected to copper clamps, through which an electric current delivered by a 10 kW power supply (maximum current  $I_{\text{MAX}} = 1300 \text{ A}$  and maximum potential  $\Delta V_{\text{MAX}} = 10 \text{ V}$ ) heats by Joule effect the Ta tube. Tantalum was chosen to build the heating system because it is an highly corrosion resistant transition metal, able to conduct heat and electricity (thermal conductivity and electrical resistivity at room temperature equal to  $57 \text{ W/(m}^\circ\text{C)}$  and  $1.34 \cdot 10^{-7} \text{ (ohm}\cdot\text{m)}$ , respectively, both increasing with temperature increase) and able to operate at very high temperatures: for the pressure of  $10^{-4} \text{ Pa}$  (that is the pressure level inside the chamber during the working conditions) Ta starts to sublime at approximately  $2200^\circ\text{C}$ . Moreover thanks to its low emissivity (0.15 at  $1000^\circ\text{C}$  and 0.26 at

2000°C), tantalum is able to screen efficiently the target box, limiting the cooling effect by thermal radiation.

The high temperature target system (composed of disks, box and heating system) is located under vacuum inside a water-cooled chamber (see figure 5.9 at paragraph 5.3): vacuum and high temperature are essential to enhance the radioactive isotopes extraction.

## 5.2 The in-target yields

The following results were obtained through several MonteCarlo calculations (MCNPX code [8,9] with the ORNL fission model) performed for the target configuration described in the previous paragraph. Numerical results turn out that a power of 0.19 kW is deposited in the window, 4.1 kW in the seven UC<sub>x</sub> disks, 1.7 kW into the three dump disks and 2.2 kW are lost outside the disks (due to proton scattering). Thus, the average power deposition for the UC<sub>x</sub> target disks is about 4.1 kW / 7 disks = 0.58 kW/disk. The energy loss and the fission yield values for the seven disks are reported in Figure 5.3.

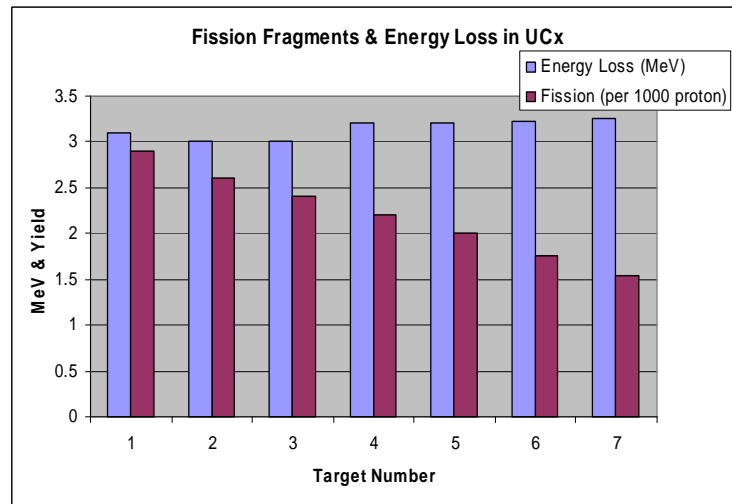


*Figure 5.3: Energy loss and number of fissions in the disks.*

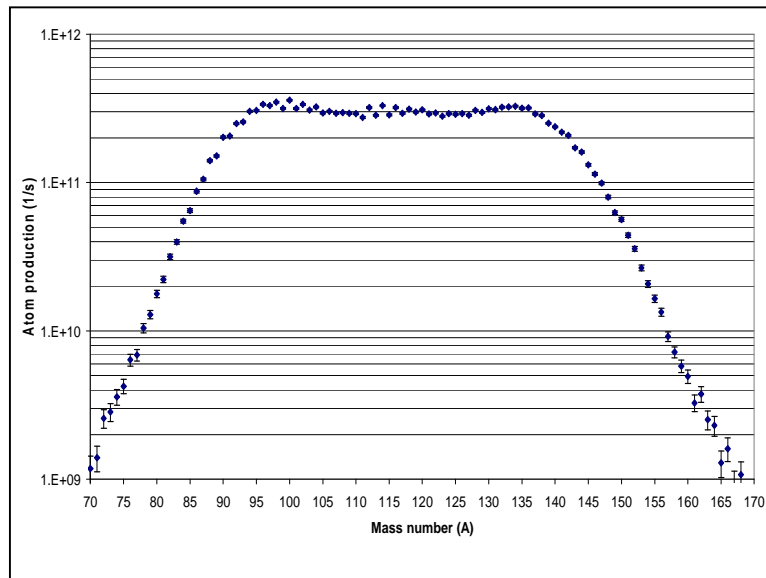


*Figure 5.4: Fission mass spectra yields.*

The total calculated fission rate in the seven disks is about  $1 \cdot 10^{13}$  fissions  $s^{-1}$ . The peak-to-valley ratio in the mass number distribution of the fission products, that is very pronounced in thermal neutron induced fissions at about  $A=115-120$ , is here only about a factor of 2 (see figure 5.4).

The isotope in-target production reaches values up to  $\sim 10^{11}$  atoms/s. The  $^{132}\text{Sn}$  isotope, being a double-magic nucleus, is one of the radioactive nuclei of interest. Its production is here estimated to be  $\sim 1 \cdot 10^9 s^{-1}$ . A more general view of the in-target yields is given in figure 5.5.

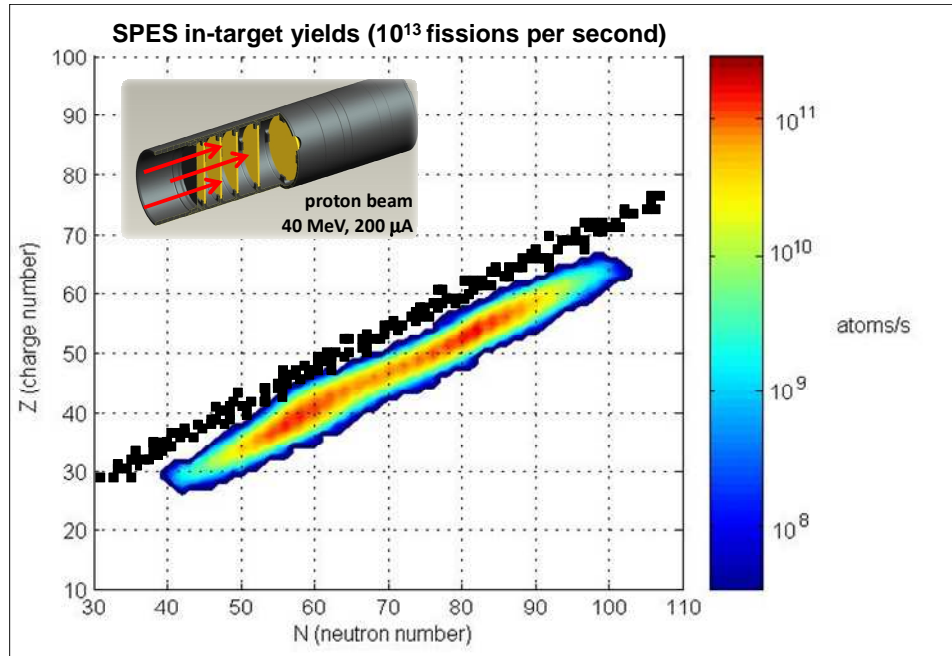


Figure 5.5: Representation (nuclide chart like) of the in-target isotope production.

### 5.3 The target thermal analysis

The power of the primary beam deposited in the target components (*i.e.* target disks, dump disks and box) is mainly due to the beam-material interaction. Due to the low pressure environment and to the high temperature of the target, this heat can be removed mainly by thermal radiation, and directed to the heat sink constituted by the vacuum chamber (see figures 5.6 and 5.9). This process can be divided into two steps: the disks that radiate heat to the box, which, in turn, transfers the heat to the chamber walls, also in this case by thermal radiation. It has to be pointed out that the box has to be held at about  $2000^{\circ}\text{C}$  for optimizing the fission product extraction; the vacuum chamber walls are kept at about room temperature.

The primary beam power deposition described in the previous sections was used as an input data in a set of numerical thermal analyses performed to study in detail the thermal behaviour of the target. In particular the target steady state temperature distribution was calculated thanks to some *ad hoc* numerical models defined using the ANSYS finite elements commercial code (see figure 5.6); the main results are presented in [6,7] and a plot of the target steady state temperature distribution is reported in figure 5.7.

With respect to the disks, the analysis was mainly devoted to evaluate the maximum temperature, in order to warrant that no melting will occur. The thermal load input data related to the primary proton beam were assigned in an accurate way, considering the variability of power density along the radial direction. The results obtained for the  $\text{UC}_x$  disks show, even in the most heated disk, a safe margin with respect to  $\text{UC}_x$  melting point. In the dump disks the temperatures are sensibly lower.

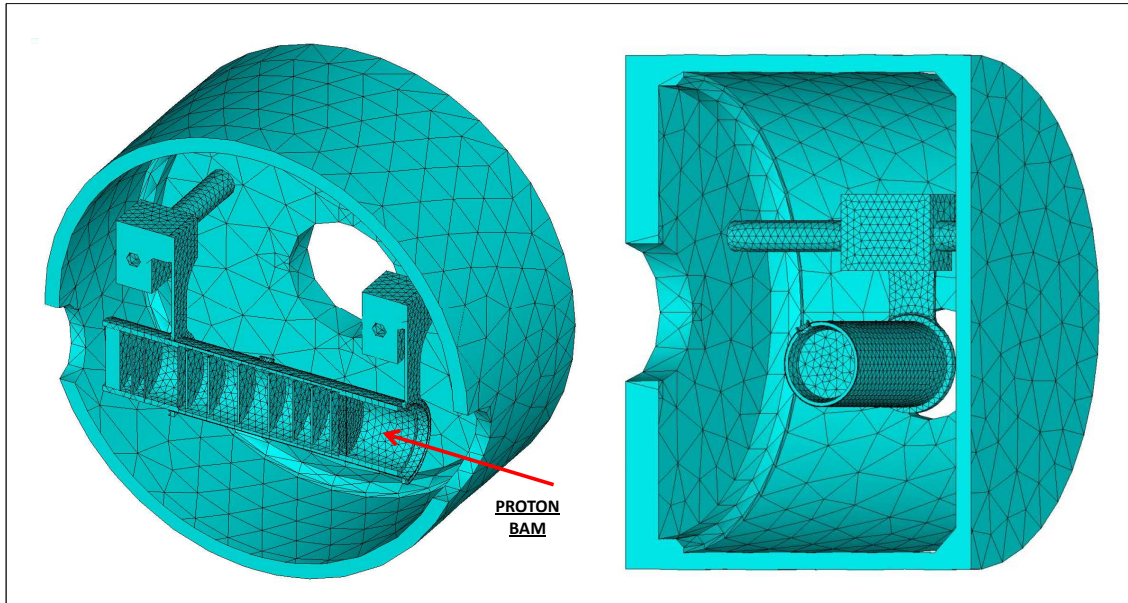


**Figure 5.6:** Section views of the FE numerical model used to simulate the thermal behaviour of the SPES target.

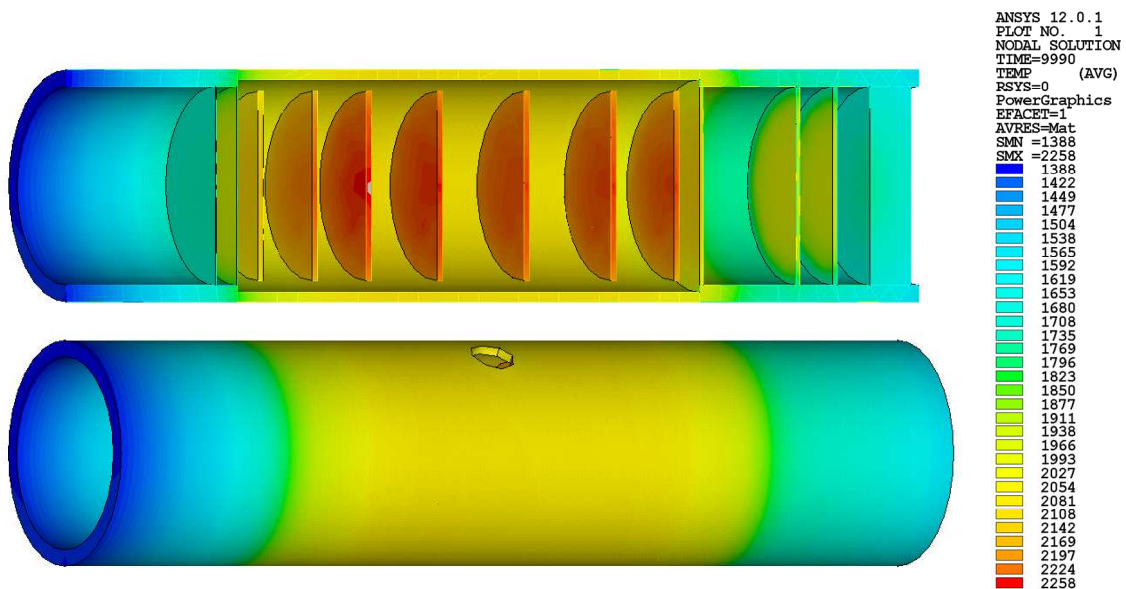


**Figure 5.7:** Temperature plot [°C] of the production target correspondent to the proton beam thermal load (results from the new FE model).

With the aim to validate calculations, an important set of experimental off-line tests was performed at LNL, in the SPES High Temperature laboratory. A full scale prototype of the SPES target (see figure 5.8) was produced, using SiC disks instead of UC<sub>x</sub> ones. It was installed with the target heating system inside the vacuum chamber and heated by Joule effect. Temperature measurements were performed (using a two-colours infrared pyrometer), showing in general a good agreement with FE calculations. Figure 5.10 reports the comparison between numerical and experimental temperatures, monitored on the external surface of the heating system's Ta tube.



**Figure 5.8:** The full scale SiC SPES target prototype.



**Figure 5.9:** Target and heating system installed in the vacuum chamber (left); the water-cooled vacuum chamber closed and ready for the high temperature test (right).

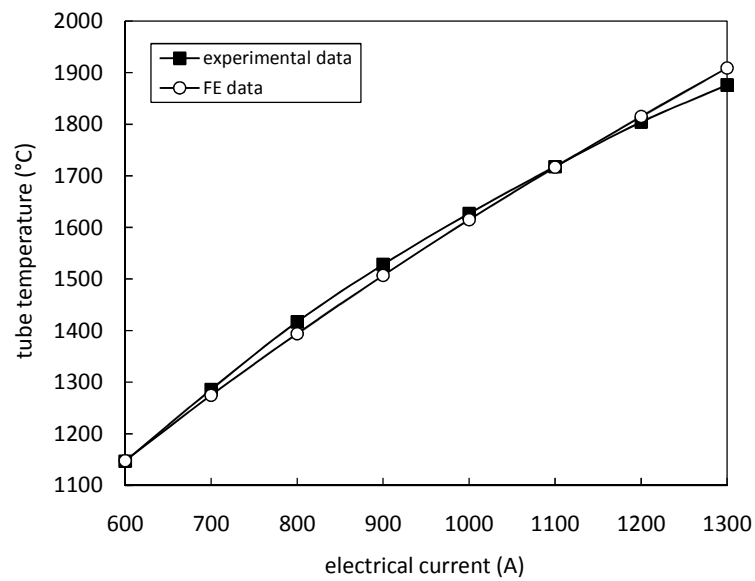


**Figure 5.10:** Comparison between numerical and experimental temperatures, monitored on the external surface of the heating system's Ta tube.

Once concluded the experimental tests with the target system only, a new set of off-line tests was performed including the SPES surface ion source, connected to the target system by means of the transfer line. Two Joule heating electrical circuits were considered: the target circuit supplied by the target heating system current, and the ion source circuit, supplied by the ion source current. In particular figure 5.11 shows the target – ion source assembly heated by an ion source current of 200A: the temperature discontinuity between the tantalum tube of the target heating system and the transfer line is evident. The aforementioned discontinuity is clearly visible also in figure 5.12 where only the target heating system (with 700A of heating current) contributes to heat the target – ion source assembly. The two objects seem to be separated, independent: the transfer line's extremity is connected to the Ta tube's hole by mechanical interference that, respect to a welded joint, does not allow to create a perfect material continuity, even if the interference is very tight. Figure 5.13 reports an image of the target – ion source assembly heated by both the heating system current (700A) and the ion source current (200A): also in this case the discontinuity at the transfer line – Ta tube connection is evident.



**Figure 5.11:** Picture of the “production target – hot-cavity ion source” assembly heated by an ion source current equal to 200A.

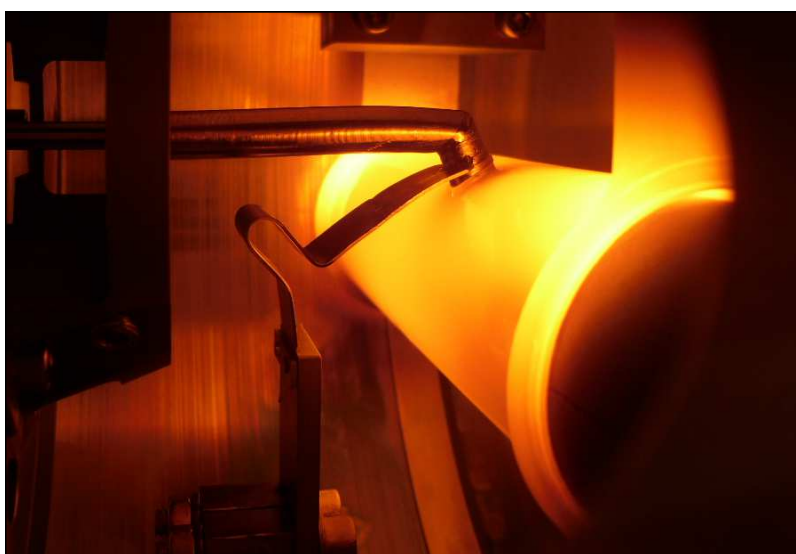


**Figure 5.12:** Picture of the “production target – hot-cavity ion source” assembly heated by a target heating system current equal to 700A.

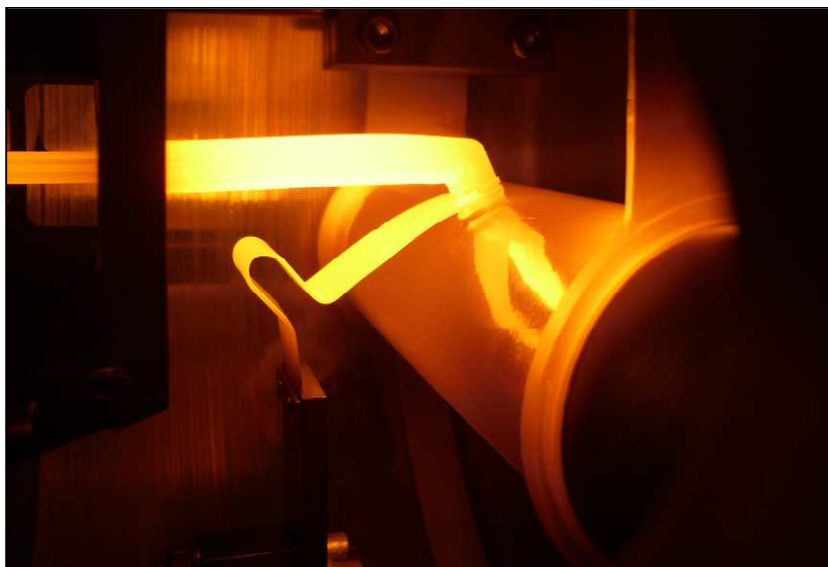


**Figure 5.13:** Picture of the “production target – hot-cavity ion source” assembly heated by a target heating system current and an ion source current equal to 700 and 200A, respectively.

#### 5.4 The target thermo-mechanical analysis

The thermal stress state of the disks was calculated taking as reference the temperature field obtained by means of the FE model described in the previous chapter. The calculation, however, was drastically simplified by the assumptions of elastic material and steady-state regime. Moreover, the  $UC_x$  physical properties are not sufficiently known and further measurements are to be carried out.

Differential thermal expansions are generated in each  $UC_x$  disk by the non-uniform temperature distribution originated from the non-uniform power deposition of the primary proton beam. The state of stress arising from such differential expansions was examined. Different approaches were attempted and they all led to similar results:

- an order-of-magnitude analysis [10];
- a numerical treatment of the equations of linear elasticity both in one- and two-dimensions [11,12];
- a numerical analysis using the ANSYS finite elements commercial code.

In this third approach, when the solution of the thermal problem was calculated (see the previous paragraph), volumes and elements belonging to the  $UC_x$  disks were selected and the thermal mesh was converted into a structural one: the structural element type SOLID45 was adopted and temperatures were input as element body loads at the nodes. The state of stress at 2000 °C, for all disks, represented by the equivalent stress  $\sigma_{eq}$  is reported in figure 5.14. The maximum equivalent stress calculated is  $\sigma_{eq} = 181$  MPa at 2000 °C. The conclusion is that the equivalent stress is lower respect to the fracture stress.

The physical parameters adopted for thermo-mechanical analyses have been found in literature [13]. The elastic modulus  $E = 215$  GPa is suggested for  $UC_x$  at room temperature, and it is put forward together with a matching value for the Poisson’s ratio  $\mu = 0.269$ . A curve for the decrease in  $E$  for  $UC_x$  between room temperature and 1500 °C has been adopted from [13] and gives  $E = 176$  GPa at 2000°C.

The mean thermal linear expansion coefficient of  $UC_x$  at 2000 °C was kept  $\alpha_m = 12.4 \cdot 10^{-6}$  °C<sup>-1</sup>. As to fracture behaviour, uranium carbide is a brittle ceramic material which may be susceptible to catastrophic fracture at low temperature, but a brittle-ductile transition is expected

to occur at some temperature in the range of 1100-1300 °C. It is assumed that, above this temperature, plasticity assures some relaxation of thermal stresses.

Fracture stress is given up to ~1300 °C only, where it is  $\sigma \approx 200$  MPa. The assumption of linearity seems rather adequate up to ~1300 °C, more questionable beyond. Therefore the study at 2000 °C can be considered as a sort of ‘best indicator’ of what happens in nominal operation.

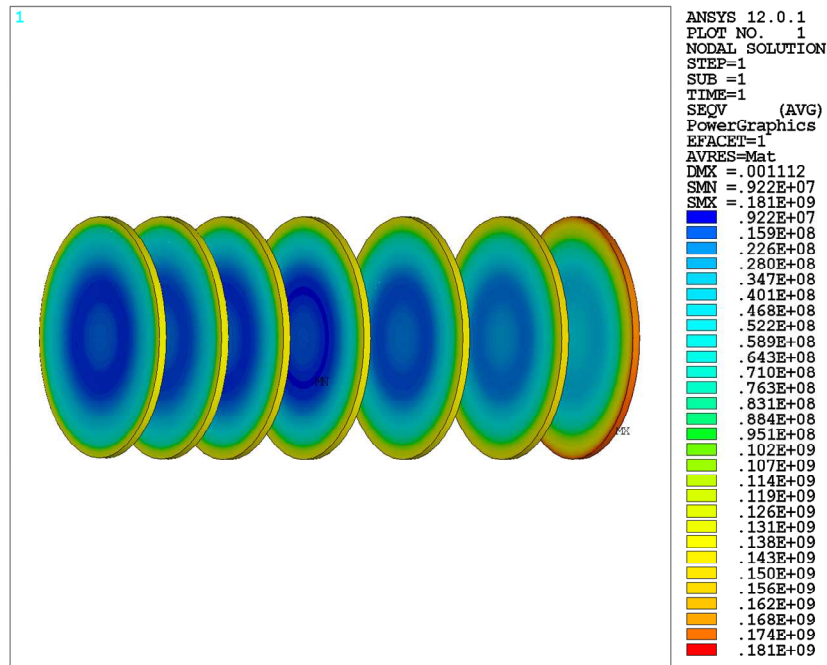


Figure 5.14: Equivalent Von Mises stress plot [Pa].

## 5.5 Release time calculations

The final intensity of a radioactive ion beam depends on the efficiency of different processes: the target production yield, the target efficiency, the ionization efficiency, the transportation efficiency along the accelerator. In order to optimize the target efficiency it is very important to minimize the time needed by the radioactive species to join the ion source.

Several simulations have been performed using the GEANT4 toolkit [14], as well as the RIBO (Radioactive Ion Beam Optimization) code [15], in order to estimate the release time for some neutron-rich nuclei. The target temperature was imposed equal to 2000°C for all the simulations. The diffusion inside the grains of the target material, the effusion in the inter-grain space and the free-effusion were taken into account. Moreover, for each collision an average adsorption-desorption time  $t_s$  (sticking time) was considered. Release time calculations were performed considering the release of the neutron rich atoms  $^{132}\text{Sn}$  and  $^{90}\text{Kr}$ .

In the calculations we assumed the SPES UC<sub>x</sub> disks being made with standard ISOLDE UC<sub>x</sub> so the ISOLDE parameters were used:

- average flight path in the powder FP = 15 μm;
- sticking time for Sn isotopes  $t_s = 10^{-6}$  s;
- diffusion time constant for Sn isotopes  $\tau_D = 1$  s;
- diffusion time constant for Kr isotopes  $\tau_D = 10$  s [16].

The average total effusion times  $t_{eff} = (0.41 \pm 0.02)$  s and  $t_{eff} = (0.22 \pm 0.02)$  s were calculated, for Sn and Kr isotopes respectively. Considering the average diffusion and effusion time the total release fraction was calculated for Sn and Kr isotopes as a function of the half-life,

as reported in figure 5.15. The final total release fraction for  $^{132}\text{Sn}$  is about 90% whereas the total release fraction for the short-lived  $^{133}\text{Sn}$  is about 40%. The total release fraction for  $^{90}\text{Kr}$  was found to be 80%.

It is clear that the diffusion time gives an important contribution to the total release time therefore it is very important to optimize the material structure of the target disks. To this purpose, an extensive study of the target materials is in progress at LNL.

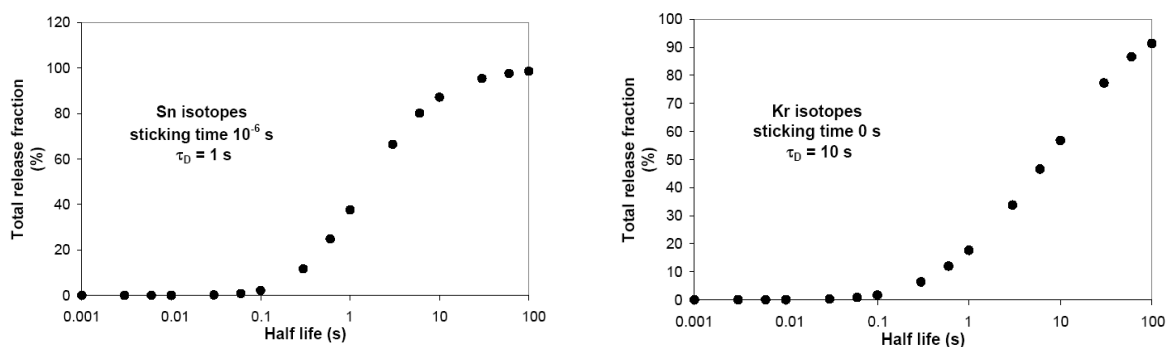


**Figure 5.15:** Calculated total release fraction for Sn and Kr isotopes produced in  $\text{UC}_x$  material.

Experimental tests to be performed at ORNL and LNL are also planned in order to validate the simulations.

## 5.6 Development of the target pellets

Radioactive Ion Beam (RIB) production is deeply affected by the characteristics of the target impinged by the proton beam. The composition and the degree of purity of the constituent materials, the microstructure and morphology (i.e. crystalline phase, grain size, porosity) of the target are of particular importance to this purpose. The kind of isotopes produced, in turn, depends both on the energy of the incident beam and on the fissile material, whereas the efficiency release is mainly related to the isotopes diffusion inside the target and to their gas-phase effusion (molecular flow plus multiple ad-desorption) [17].

Both the diffusion and effusion of the radioactive species in/from the target strongly increase with the increase of the temperature. For this reason the target working temperature must be kept as high as possible, in order to grant atoms release faster than their decay. On the other hand, the working temperature of the target is limited by the vapour pressure of the target constituents, by the temperature stability of the target material and by possible reactions which may occur between the target and the target holder at high temperature. For these reasons, refractory compounds like carbides and oxides have to be used as target materials in order to sustain these conditions.

### 5.6.1 The Pellet Production

Three main routes are nowadays available for the production of porous materials:

- a) the replica technique: a polymeric sponge is impregnated by slurry of appropriate composition, the system is then dried and the polymeric sponge burnt-off;
- b) the direct foaming technique: a foaming agent is introduced into a suspension of appropriate composition;
- c) the sacrificial templates technique: a sacrificial component with selectable shape and size is introduced in the system and then burnt-off, leaving empty spaces.

Mixtures of uranium oxide and graphite at high temperature showed particularly favourable release characteristics for many isotopes [18-20]. In particular, the uranium carbide can be produced by reaction of a precursor (metal oxide) with a carbon based matrix (graphite powder or low density carbon foam generators) according to equation 1.

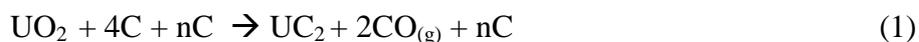


*Figure 5.16: The high temperature furnace for UC<sub>x</sub> production assembled at LNL.*

This is due to the fact that working in excess of graphite results as an improvement of the release efficiency, issue very important in the ISOL-RIB target application. Therefore, the carbides of lanthanum and uranium produced by this reaction, or LaC<sub>2</sub> and UC<sub>2</sub> are commonly referred to by LaC<sub>x</sub> and UC<sub>x</sub>, indicating that they will be composed of carbide and carbon residue.

The formation of uranium carbide occurs under high vacuum at temperatures ranging from 1100 to 1400 °C. The gas released during carbo-thermal reduction (CO in eq. 1) is responsible for pores formation. Open porosity (interconnected structure) was demonstrated to improve isotope release [21]. Moreover, in order to obtain materials withstanding the extreme working conditions, sintering of the composite powder is a successive, necessary, step achieved at temperatures even higher than 1700 °C.

The preparation of SPES samples for thermal treatment follows the classic procedure for the production of ceramics from powders: precursors are initially mixed manually or using a mill, and then add a binder (typically polymer). Without this, the resulting powder is cold-pressed for enough time to write a pre-sintering of the mixture, allowing for the extraction from the die-

pressing without compromising mechanical stability. The samples thus obtained are subjected to heat treatment of carburization in an high vacuum - high temperature furnace (see figure 5.16).

According to the SPES steering committee guidelines, the development of tailored  $UC_x$  disks will follow the scheme reported in figure 5.17.

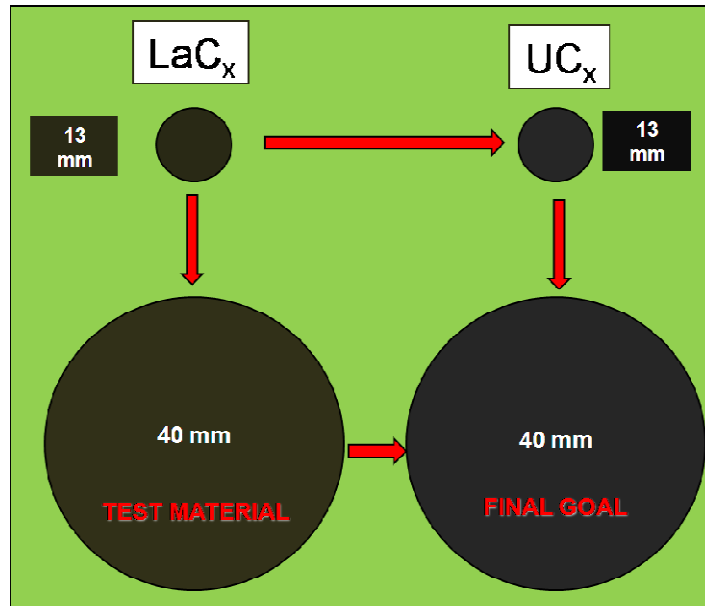


**Figure 5.17:** Schematic overview of the R&D on the development of 40 mm  $UC_x$  disks.

The processing route followed to produced  $LaC_x$  and  $UC_x$  13 and 40 mm thin disks consists of 3 steps, as reported in figure 5.17. As can be observed in Figure 5.18, the critical points of process transfer from 13 mm to 40 mm disks are related to the larger amount of reagents (metal oxide and graphite) involved in the reaction. The technological troubles that arise from this point can be divided into two categories:

- The first one is related to the instruments to be used for the three process steps (mixing and grinding (1), pressing (2), carburization and sintering (3));
- The second is related to safety and in other words to the compatibility of such techniques to the production of radioactive materials.

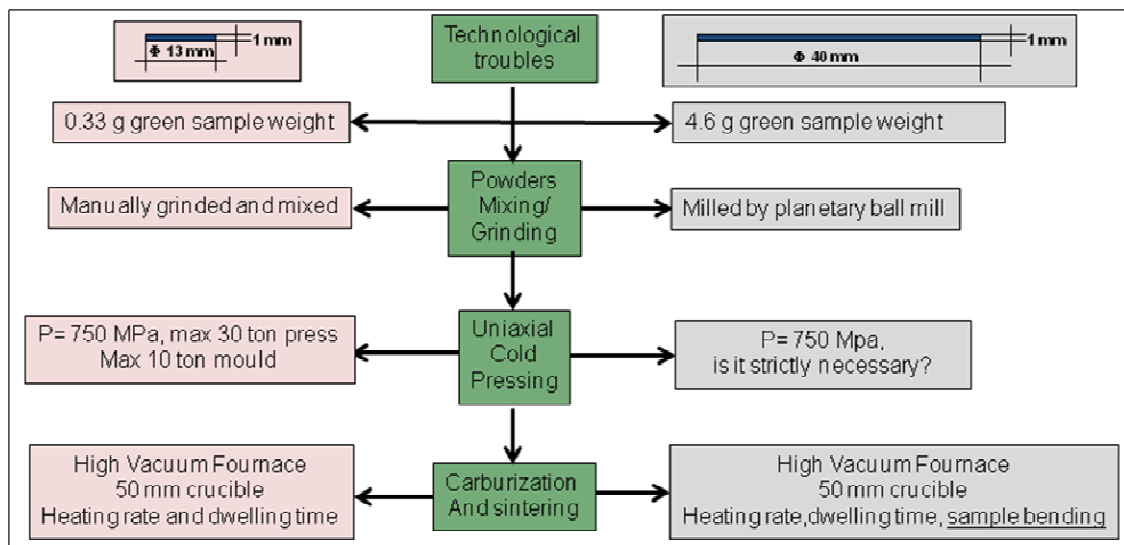


**Figure 5.18:** Process scheme and critical points.

Handling radioactive material (even if of low activity like depleted uranium) requires special precautions, authorizations, and dedicated radiological controlled area to avoid workers and instruments contamination. Two production lines for 13-mm and 40-mm diameter pellets have been developed.

The thermal processes are performed in two different furnaces, depending on whether it is requested to produce samples for testing the reactivity of the components (prototype discs, 13 mm of diameter) or samples of the final size required by the SPES target (reference discs, 40 mm of diameter). In the first case, the carburization and the subsequent sintering processes are performed in a dedicated furnace located in the Department of Chemistry of Padova University (see figure 5.16), which allows to reach maximum temperatures of about 2100 °C in high vacuum ( $\sim 10^{-6}$  mbar).

Working at very low pressures facilitates the reactivity of the components and, in the same time, prevents the rapid oxidation of the carbide which would undermine stability. The main part of the furnace consists of a bell-shaped vacuum chamber containing a graphite crucible heated by Joule effect using a power supply capable of providing the maximum voltage of 10V and the maximum current of 1000A.

To reach the temperature levels needed for the carburization of the oxides and for the sintering of carbides, a dedicated screening system, designed and built at LNL, was installed around the crucible. The following figure shows the  $UC_x$  furnace and its main components.



*Figure 5.19: Graphite crucible (left) and screening system (right).*

The crucible (represented in figure 5.19) allows the carburization of the sample placed within it in a horizontal position, and therefore the treatment performed in this oven is called "horizontal carburization".

In the case where we want to produce samples according the SPES standard diameter of 40 mm, the furnace used, entirely designed and built at the Legnaro Laboratories, is quite different than the previous one. In this case the oven system looks like the on-line SPES target heating complex. The furnace vacuum chamber in this case consists of a hollow cylinder of stainless steel mounted on a guide to allow easy opening and closing, as reported in Fig 5.20.

The stainless steel chamber which houses the tantalum heater with size similar to the SPES target, is connected to two current terminals of copper associated with the power supply system. Inside the Ta heater a cylindrical graphite box is positioned, containing the samples that will be thermal treated.

The heating chamber is equipped with a dedicated screening system (see figure 5.21), which allows to reach the temperatures required for carburization and sintering heat treatments (more than 2100°C).



**Figure 5.20:** The LNL furnace for the production of carbides of diameter 40 mm.

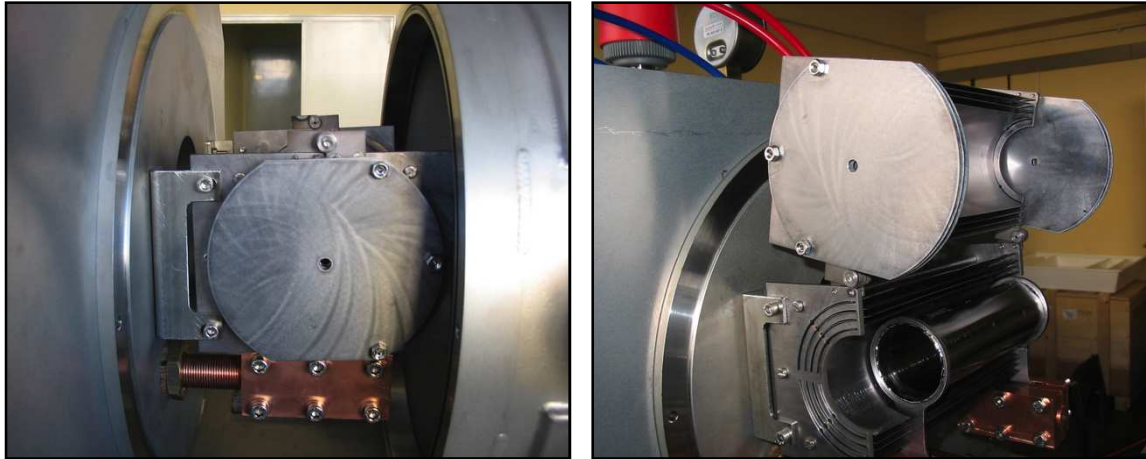


**Figure 5.21:** Closed screening system (left) and open screening system (right).



**Figure 5.22:** The 40 mm UC<sub>x</sub> pellet (1 mm thick) after thermal treatment (the average bulk density is about 3 g/cm<sup>3</sup>).

### 5.6.2 The Pellet Characterization

The final target sample features are influenced by many physical, chemical and structural properties (i.e. purity degree, grain size, porosity). In spite of research on the development of suitable targets, going back several decades, a complete knowledge of the influence of the production processes of the targets on all these features and on the RIB production has not yet been fully achieved. Therefore a careful characterization of the features of the produced pellets represents a primary purpose for developing suitable and reproducible targets. The main goal in this R&D activity is to design a standard procedure aimed to the production of uranium carbide-based pellets with the best *online* performances.

This can be achieved, by a careful characterization process of prepared pellets in order to optimize the thermal treatment of several oxide and graphite mixtures, in different ratio and with dimensions ranging from nano- to micro-meters. In addition, similar procedures and

characterizations will be extended to new promising porous, low-density ceramic materials ( $UC_x$  or  $LaC_x$  foams).

So the final step of the R&D on SPES material development consists on the pellet characterization stage. In fact, after the heating treatment, some pellets has been designed to have a characterization process which consists mainly of Differential Scanning Calorimetry (DSC) analysis performed on the starting mixture the X-Ray Diffractometer (XRD) and, finally, the SEM-EDS investigations of samples carburized and sintered at different temperatures (see figure 5.23).

Following the route showed, several  $UC_x$  samples, with controlled amount of porosity and tailored emissivity, is under development. As reported in figure 5.24, XRD analyses show the formation of tetragonal  $UC_2$  and graphite. A minor amount of a secondary U-C phase was also formed up on carburization and sintering. Samples possessing a bulk density of about  $3 \text{ g/cm}^3$  and grain size less than  $1 \mu\text{m}$  have been produced in the Padua University  $UC_x$  laboratory.



**Figure 5.23:** (A) Scanning Electronic Microscope (SEM); (B) X-ray diffractometer (XRD); (C) TG/DSC thermal instrument.

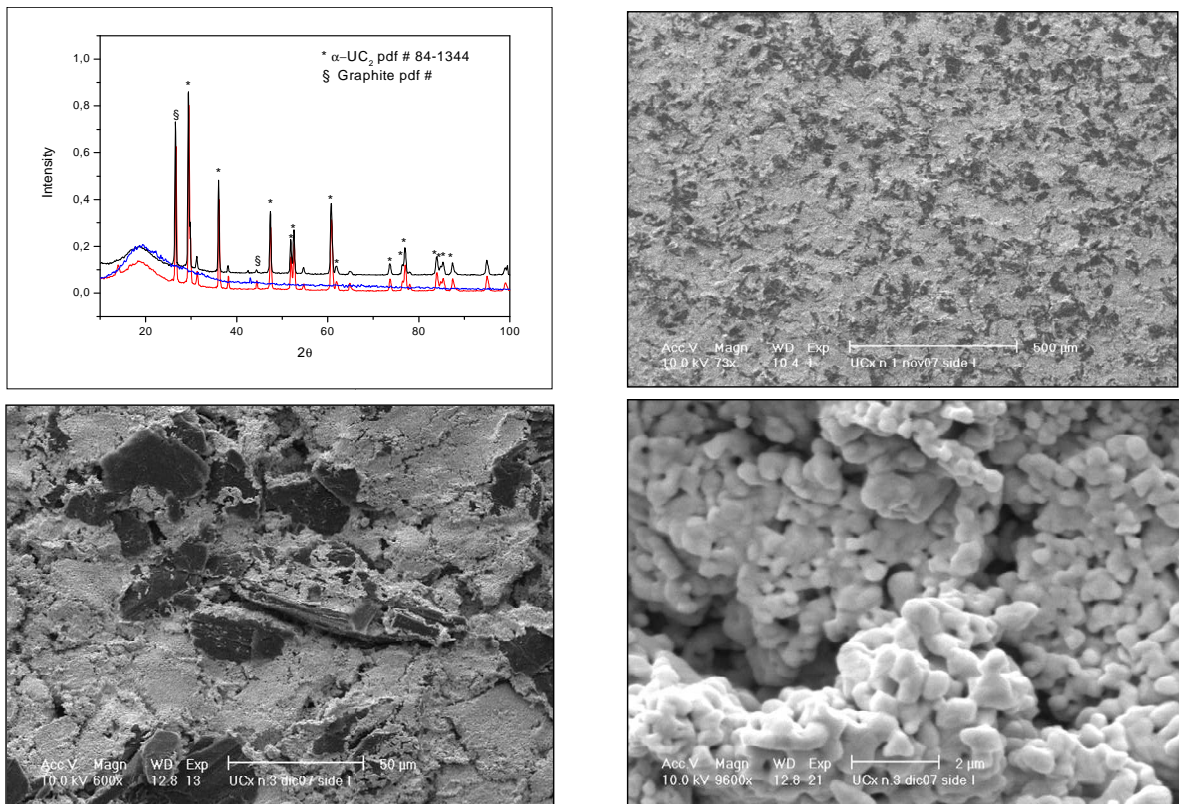


**Figure 5.24:** SEM analysis of  $UC_x$  target at different magnification and XRD (left upper) after carburization and sintering.

In the future the production of UC<sub>x</sub> pellets with different techniques will be employed to change the sample porosity (from <10 %, dense target, to 70-80%, typical value of foams) and the pore dimensions and shape (spheroidal, acicular). In particular, the porosity will be realized either by means of sacrificial fillers (PMMA based micro-spheres that decompose completely during the thermal treatment) or by direct foaming methods (mixing the raw materials with a low-temperature evaporation solvent) or with the replica technique (polymeric foams covered by ceramic powder and treated at high temperatures).

In this way, it will be possible to acquire the necessary know-how to control not only the shape and dimensions of the pores but also their morphological characteristics. In fact the passage from a closed to an open structure would significantly improve the target permeability. All the correlations between the observed effusion properties of the *on line* targets and their structural properties will be exploited in order to improve technology of the pellet production.

### 5.6.3 Emissivity and thermal conductivity measurements

At the working temperature of an ISOL target (2000°C), thermal radiation, mainly, and thermal conduction control the target heat dissipation and the target temperature field.

Since the amount of radiative heat transfer is calculated by temperature, emissivity and geometry of the target, emissivity as well as temperature measurements are very important for preliminary studies and calculations. Therefore it is often required to directly measure the emissivity and the conductivity for a given material, under the real conditions since significative variations values may occur. The experimental set-up built at LNL-INFN and used for thermal characterization of the SPES samples is reported in Figure 5.25. A power supply ( $I_{\max}= 1000$  A and  $V_{\max}= 10$  V) directly heats by Joule effect a graphite crucible connected to copper clamps. Heat is shielded by Tantalum foils symmetrically distributed around the crucible. Vacuum is supplied by a diffusion and rotary pump in series.

The system is capable to reach a temperature as high as 2100 °C and vacuum up to  $10^{-6}$  mbar. Temperature is measured by a double frequency pyrometer. The pyrometer has a temperature range of 1000-3000 °C and the wavelength ranges are respectively 0.85-1.05  $\mu\text{m}$  and 1-1.10  $\mu\text{m}$ .

Concerning the emissivity measurements, up to the present several methods have been performed using various detectors such as IR spectrometer, a radiometer and an infrared pyrometer.

In the framework of the R&D of SPES target a direct method for emissivity measurements upon heating in the range 1000- 2000 °C under vacuum is working at SPES laboratory. The method consists on the use of a dual frequency pyrometer put above to the sample surface. Once temperature has been measured in bi-chromatic mode, emissivity can be calculated from the Stefan-Boltzmann law with the pyrometer in mono-chromatic mode.



*Figure 5.25: The LNL furnace for pellet thermal characterization.*

The pyrometer is settled in a direction normal to the sample and the radiation passes through a boro-silicate glass window almost completely transparent to infrared radiation for the wavelength band of the instrument adopted to measure temperature. Different kinds of commercially available SiC and isotropic graphite samples were tested. In Figure 5.26 the  $UC_x$  emissivity, is reported.

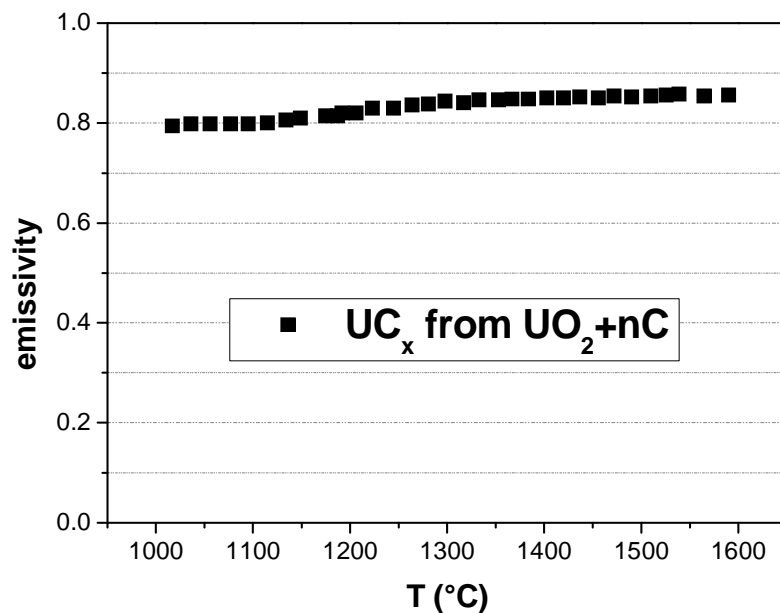


*Figure 5.26: Emissivity behaviour of the SPES  $UC_x$  pellet.*

Concerning the thermal conductivity measurements a new method has been developed at LNL. The thermal conductivity  $\lambda$  is determined by quantifying the radiation flux emitted from a heated sample in steady-state thermal equilibrium. The steady-state direct method performed at LNL overcomes this problem by quantifying the radiation heat flux emitted from a sample heated by a graphite crucible. The  $\lambda$  is determined by a linear integration of the heat flow

equation for a sample with a cylindrical geometry. For thermally insulated samples, with no internal heat sources, and a geometric symmetry along the gradient axis, the formula for heat flow is well known.

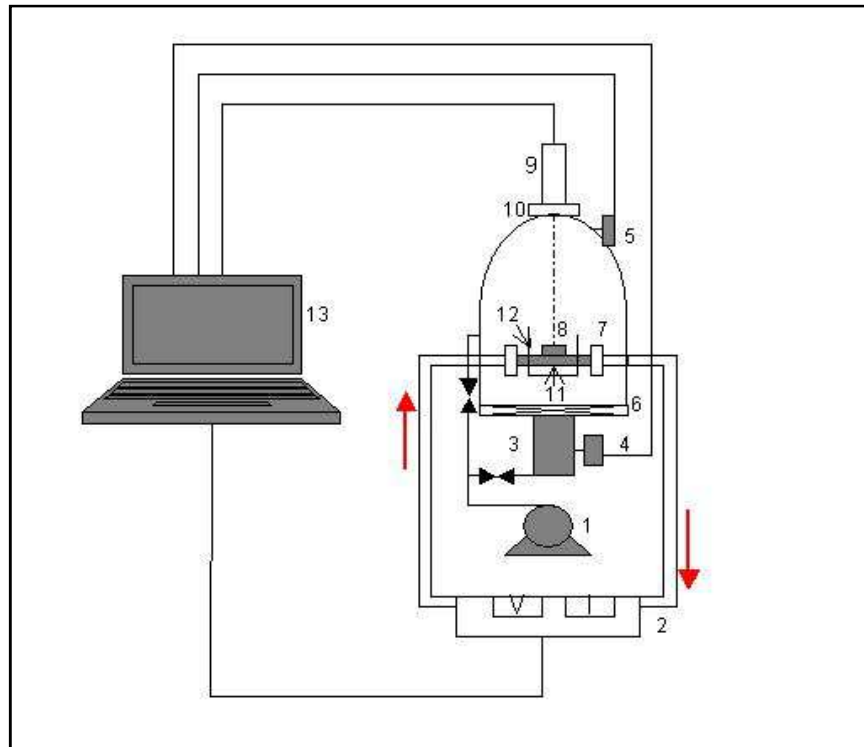


*Figure 5.27: The experimental set-up.*

Once the sample has reached steady-state thermal equilibrium with a corresponding uniform thermal flux along its axial direction, the radiation exchanged between the cold surface of the sample and its colder environment is directly proportional to the heat flow inside the sample. This is facilitated experimentally by exposing the cold sample surface to a water-cooled stainless steel vacuum bell that acts as a constant colder heat sink. The radiation flux is determined by direct temperature and emissivity measurements using a two-wavelength optical pyrometer.

## **5.7 The target – ion source system and the related experimental apparatus**

### *5.7.1 The target - ion source system*

We have adapted the engineering principles embodied in the target - ion source systems used in the HRIBF and ISOLDE facilities for remote and safe handling [22]. The attractive features of this approach is that loose contamination is enclosed in a relatively compact system.

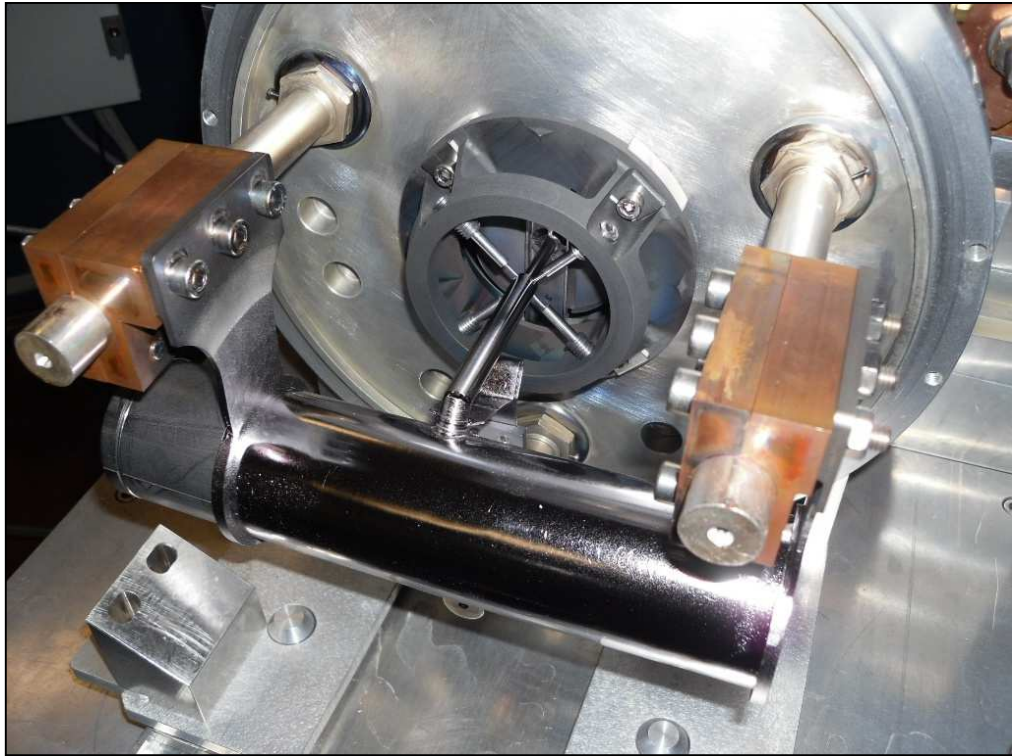


**Figure 5.28:** *The target – ion source system connected to the vacuum chamber unit.*

The SPES target unit is composed of a graphite box containing the  $UC_x$  disks, windows and dumper disks (all made of graphite), and is contained in a tantalum cylinder which is resistively heated by passing a high current through it in addition to the heat supplied by the irradiating beam. A small tantalum tube, called transfer line tube, connects the target unit to the ion source in order to plug in several kinds of ion sources (see figure 5.28).

#### *5.7.2 The SPES target chamber*

In the context of the SPES facility the target chamber is used to contain and support the target – ion source complex in an high vacuum environment, providing both the water for the cooling system and the electrical current needed to heat by Joule effect the production target and the ion source; we recall that the target – ion source complex constitutes the core of the facility and is used to convert the stable primary proton beam (PPB) into a radioactive ion beam (RIB) (see figures 5.29 and 5.30). The target chamber, with the target – ion source system inside, will be irradiated by the primary beam for approximately fifteen days; once completed the irradiation phase the chamber and the components contained, all characterized by an important radiation dose, will be removed by a remote automatic handling system (see the following paragraph). With the aim to facilitate the handling operations the chamber was accurately design including fast mechanical, electrical and hydraulic couplings.

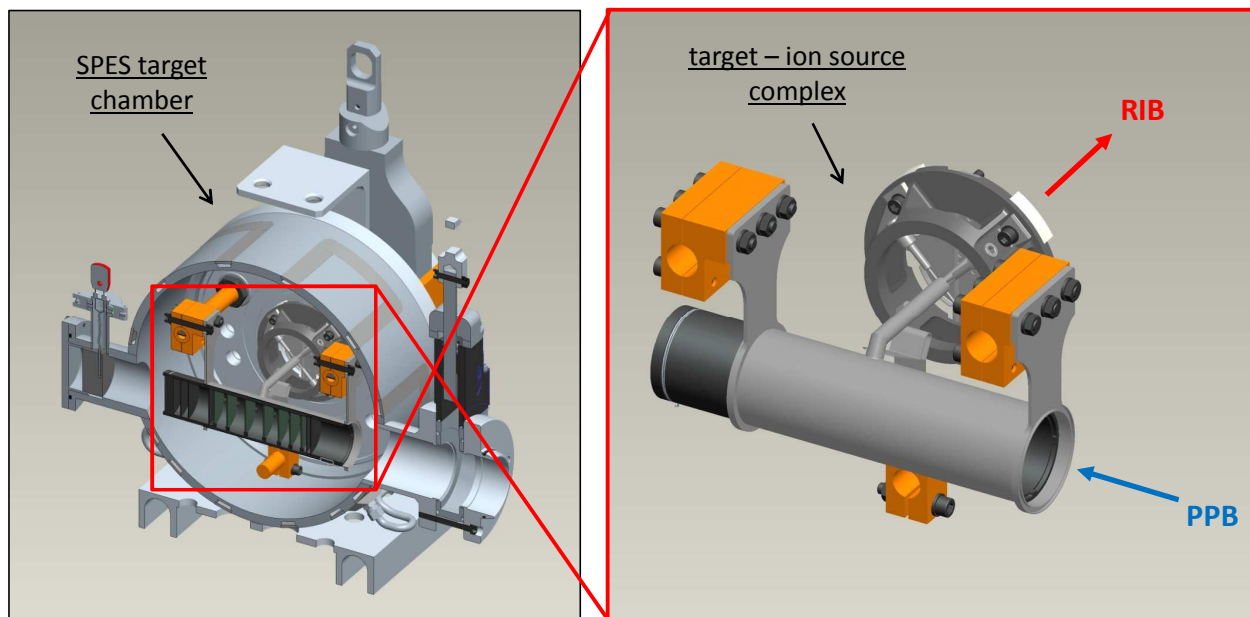


**Figure 5.29:** The SPES target chamber and the target – ion source complex.

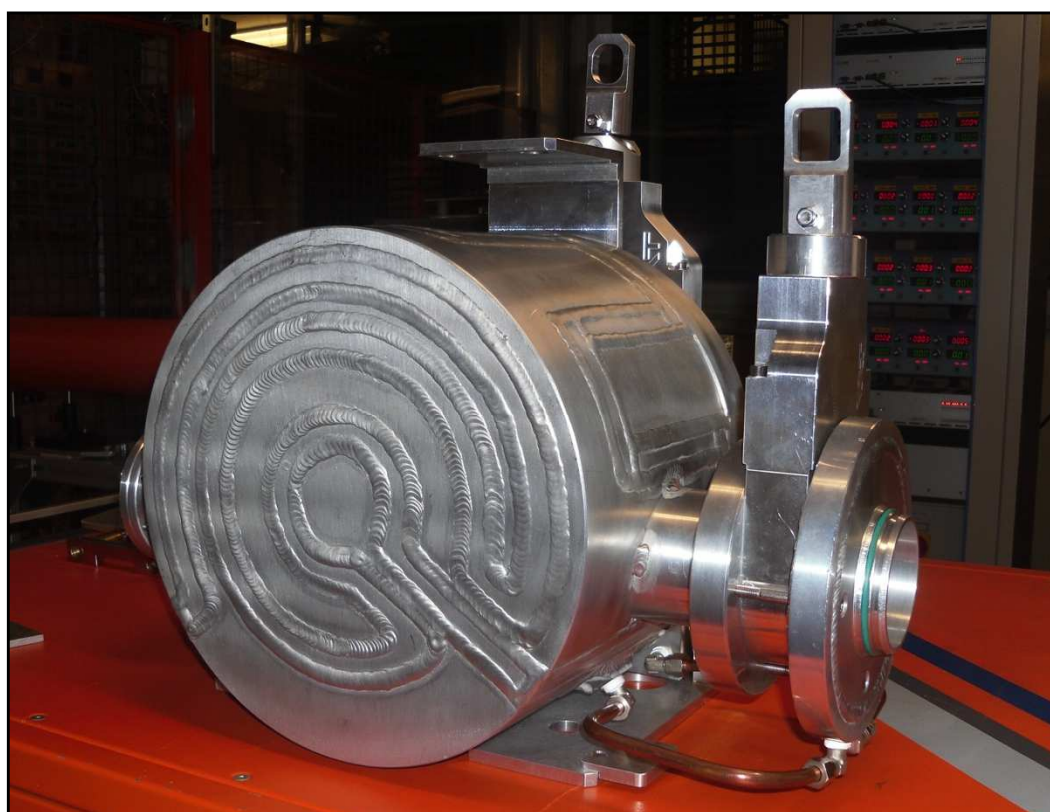


**Figure 5.30:** Picture of the SPES target chamber.

### 5.7.3 The SPES front end

The SPES production area (see figure 5.31) is constituted by the production target (that with the transfer line composes the target block), the ion source (in this chapter we will take into consideration the surface ion source or hot-cavity ion source) and all the experimental apparatus needed for their functioning that is the target chamber and in particular the front end.

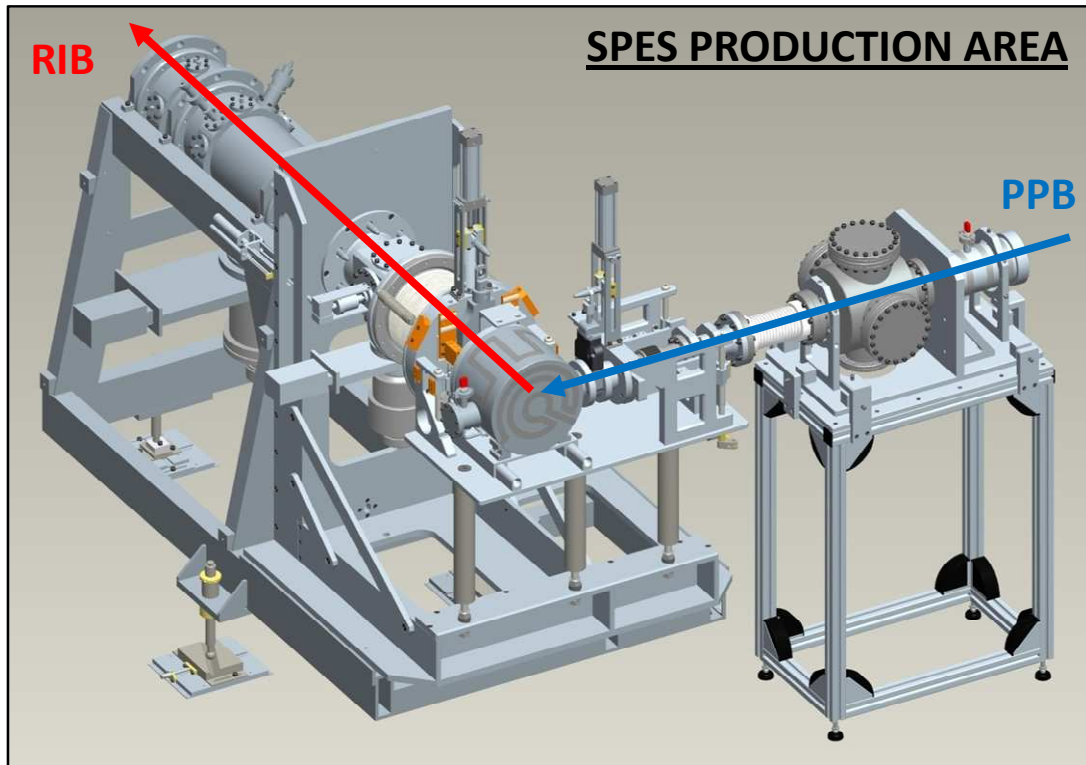


*Figure 5.31: The SPES production area.*

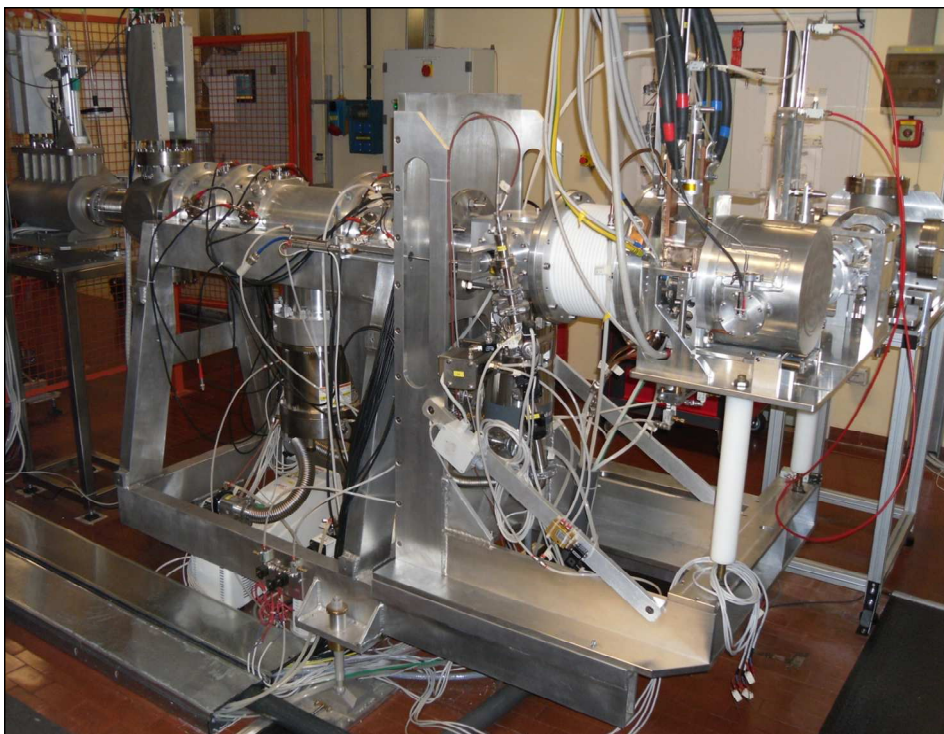


*Figure 5.32. Picture of the SPES production area prototype built at Legnaro National Laboratories.*

The SPES front end is a sophisticated experimental apparatus whose construction was based on the experience of important European ISOL facilities; its main functions are:

- to guarantee a stable positioning of the target chamber containing both the target block and the surface ion source;
- to provide high vacuum inside the target chamber, water to cool it down and electrical power to heat by Joule effect both the target block and the surface ion source;
- to allow the entrance of the primary proton beam (PPB) directed to the target block;
- to extract the radioactive ion beam (RIB) from the “target block – surface ion source” complex and accelerate it to the subsequent areas of the facility;
- to provide high vacuum both in the primary proton beam and in the radioactive ion beam channels.

The front end used in the context of the SPES project is an evolution of the front end 6 developed at ISOLDE (CERN). Respect to its precursor in the SPES front end a channel kept under high vacuum was added to allow the entrance of the primary proton beam: in fact respect to the ISOLDE facility in the SPES one the energy of the proton beam is sensibly lower (40 MeV respect to the energy level of approximately 1 GeV that characterizes the ISOLDE proton beam) and consequently it cannot impinge the target passing through air.

Then, with the aim to support maintenance operations, the front end general assembly, indicated by the code *ST\_FE000* (according to the codification scheme defined for the SPES project), was divided in two portions: the removable part (subassembly *ST\_FE200*) and the fixed part (subassemblies *ST\_FE100* and *ST\_FE300*) (see figure 5.33). The former, lying close to the target block, receives a big dose of radiation whereas the latter is more distant and its absorbed dose is sensibly lower; as a consequence subassembly *ST\_FE200* needs to be removed approximately every seven years because of material degradation while the subassemblies *ST\_FE100* and *ST\_FE300* (constituting the fixed part of the front end) are not subjected to important damages due to radiations and can last much more time. The front end was accurately designed in order to allow an easy and fast removal of subassembly *ST\_FE200*.

In this apparatus most of the components are made of aluminum alloy (low density) in order to minimize the material activation as consequence of the huge production of neutrons coming from the production target.

The most important and sophisticated section of the front end is surely the radioactive beam channel: once produced the radioactive isotopes in the target and ionized them thanks to the ion source, the radioactive ions are accelerated by a 60 kV potential difference produced between the ion source and the extraction electrode of the front end. After this stage the beam will pass through the deflector system which consists of four electrostatic steerers: by tuning the electric field of the steerers, it is possible to modify the position of the beam in the transverse plane. The next stage of the radioactive channel of the front end consists of a triplet of electrostatic quadruples responsible for bringing, by changing the values of the electric field, a focus in a desired downstream point.

Once passed through the radioactive beam channel the radioactive ion beam is directed to the beam transport area and then to the post accelerator.

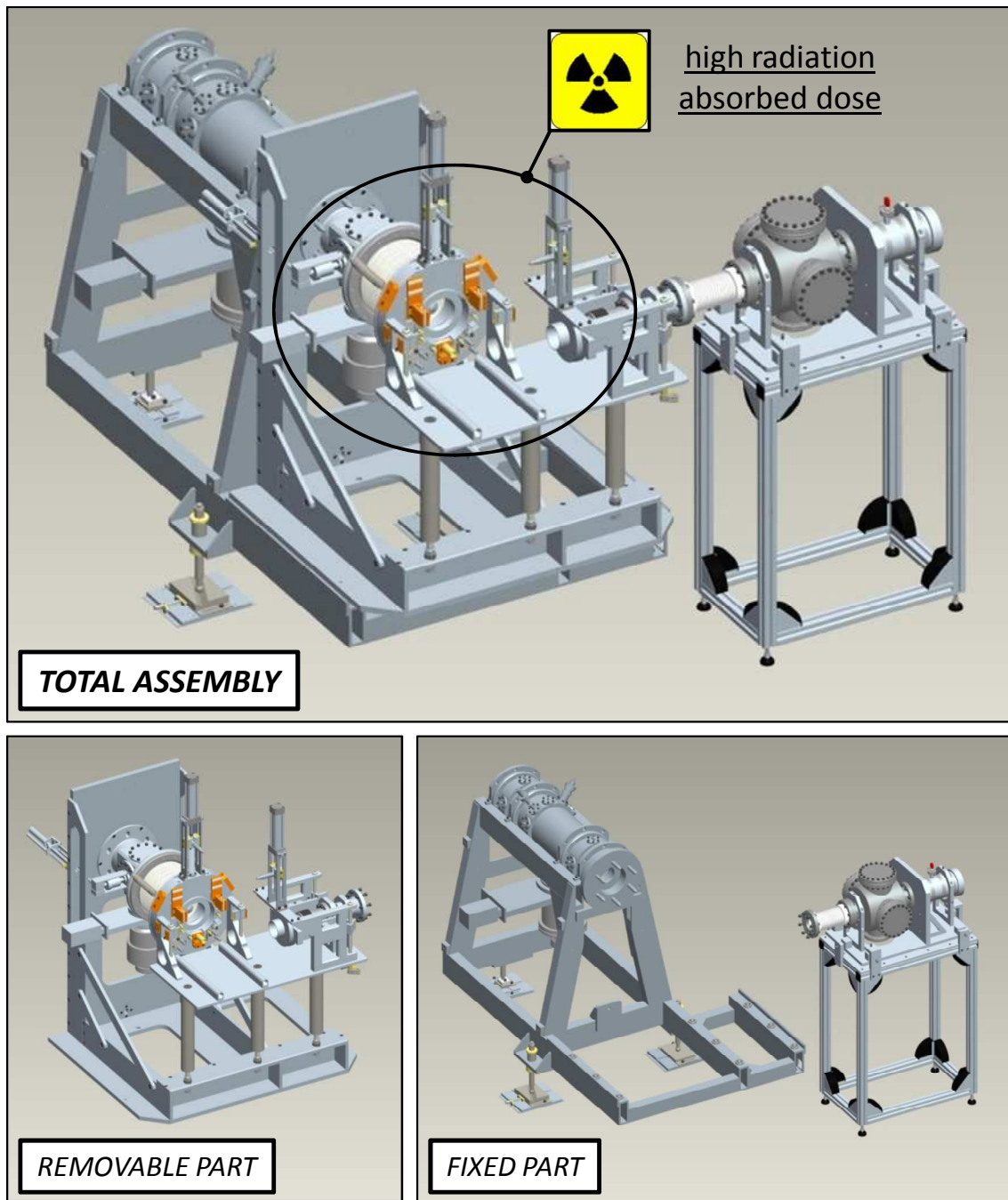


*Figure 5.33: The SPES Front-End.*

## 5.8 The target chamber Handling

The SPES Target handling is a delicate and complex action, complicated by the high degree of radioactivity reached the target after irradiation. In order to improve the security features and possibilities of intervention on the target we chose to prepare two types of movements: a vertical and horizontal. For both handling of cases, the target handling has been divided into two main, and specular, sequences:

- 1: the loading phase;
- 2: the unloading phase.

The SPES target-production chamber must be easily removed ( for servicing or storage) from both beam lines after the irradiation process. For this reason, the mechanical design of the SPES target chamber strongly takes into account this effect. The target chamber unit is coupled to the proton driver and to the RIB's beam by means of quick connectors. Since the target could be used several times, it will be shipped into a dedicated box with lead walls of 2 cm thickness.

The lead box containing the target chamber will be housed in a special repository along with other exhausted boxes waiting for the radiation level reaches acceptable values, allowing subsequent phases of disposal and possible recycling. The time required to the target materials of exhaust their dangerousness, is around two years.

Two independent devices are designed for the target chamber handling in the horizontal and vertical directions.

Recently, the handling procedures have been tested, in the SPES laboratory, using prototypes, in order to check the fitting system of the target chamber (figure 5.17) to the front-end apparatus.

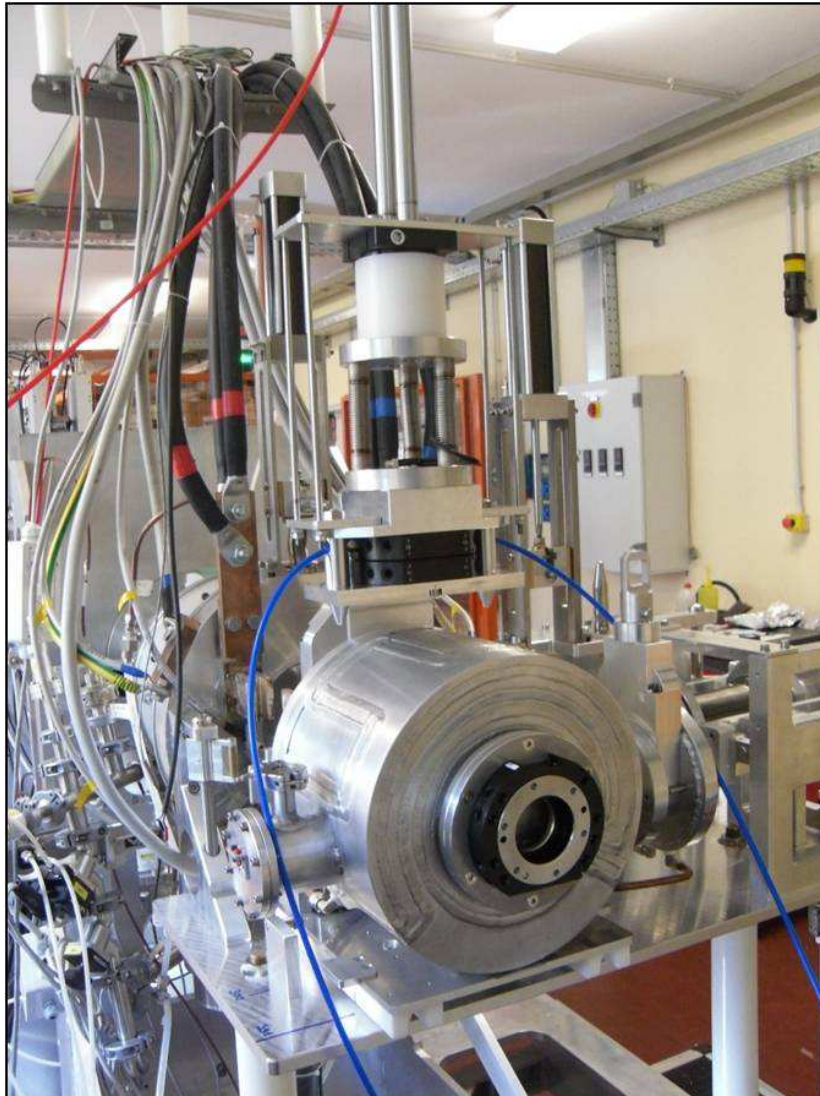


*Fig. 5.17. The SPES target chamber complex during the handling test performed at LNL.*

The handling system must be designed in order to send (and remove) the target chamber, of about 40 kg weight, into the irradiation area, where the target will be hit by the proton beam. Figure 5.18. shows the proposed handling layout, composed by two different devices, both of which operate in two different halls.

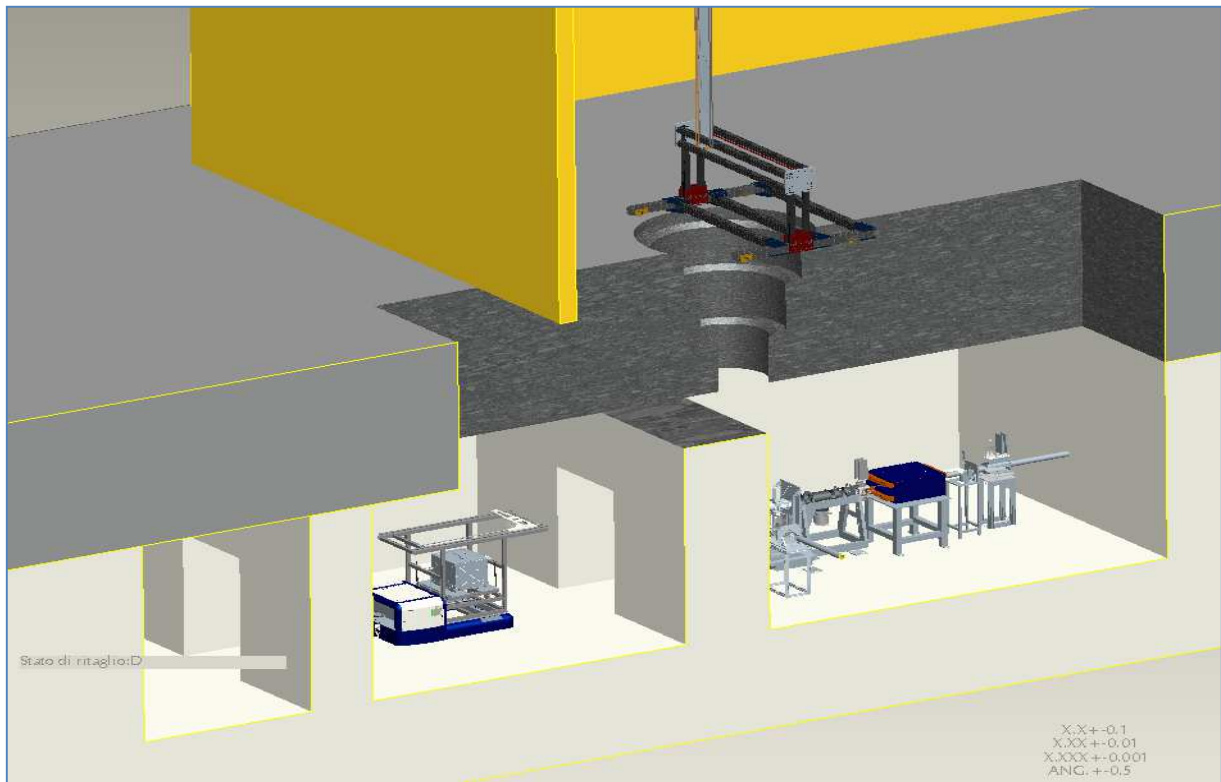


*Fig. 5.18. Layout of the SPES target chamber handling system.*

### **A) The Horizontal handling system**

For the horizontal handling system, the first phase is to carry, through the use of a trans-pallet, the target chamber, previously inserted into a box with walls of lead, inside the room dedicated to handling where there is the vehicle (Fig. 5.19).

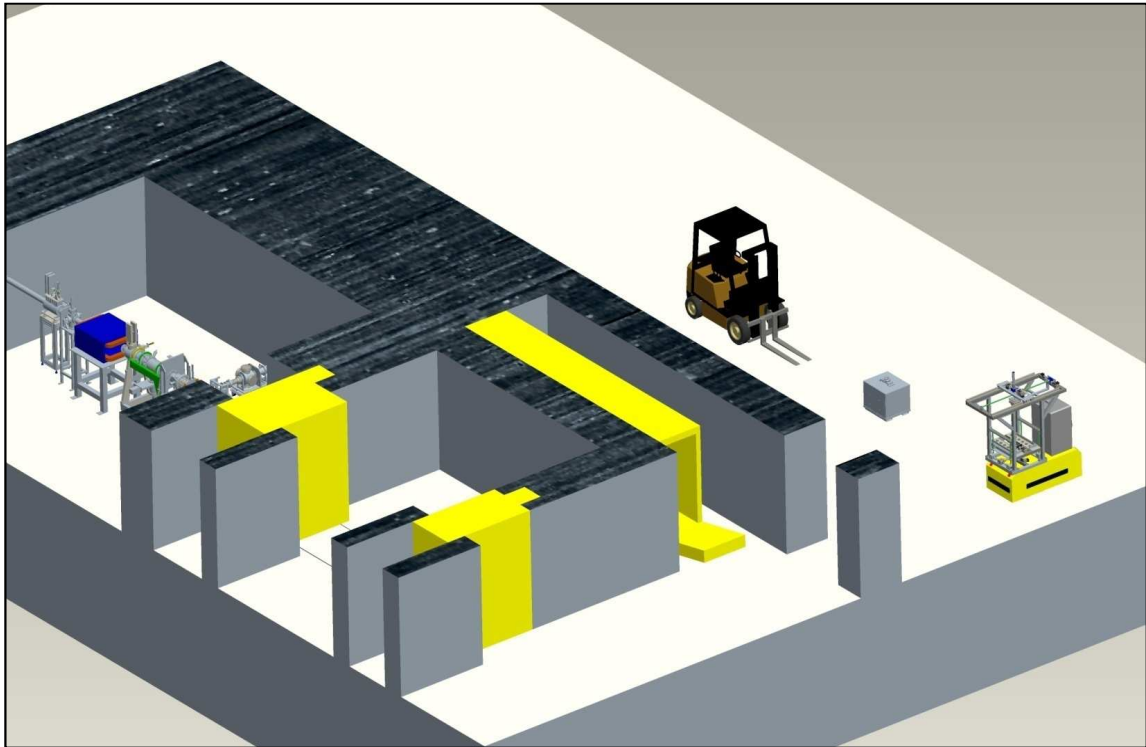


*Fig. 5.19.- Transport of the 'sarcophagus' lead chamber containing the target to the handling vehicle.*

To transport the target chamber from the deposit to the FE, it has been decided to use an AGV (Automatic Guide Vehicle). The vehicle can travel following an imposed path with extremely reduce position errors. The main duty of this kind of vehicle will be the target chamber delivery from the chamber deposit to the FE coupling table, where the target chamber will be connected to the overall system.

To automatically perform the pathway, the AGV will have optical sensors in order to monitor its position respect to a painted line onto the floor. Beside optical line monitoring as primary driving system, possible solutions will be chosen among magnetic lines and laser distance driving. These kinds of solutions, even if it is more cost expensive rather than a fixed rail, allows more flexibility and a complete isolation of the bunker when all the doors will be hermetically closed, due to the absence of holes for the rail.

Additionally, it will be possible to change the mode of operation from automatic to manual where cameras on the AVG and a remote joystick will allow a human operator to control the vehicle. This redundancy on the control system is intended to ensure a minimal fault rate.

In order to place the target chamber inside and outside the vehicle, a series of mechanical devices placed on top of the AVG will be used (figure 5.20.). The system includes a series of sequential operations: positioning of the lead box inside the vehicle, removing the lid of the box, taking the target chamber unit from the box by using a dedicate interface tool and placing it onto the FE coupling table. The moving operations are carried out by screw systems, driven by electric motors controlled by means of PLC devices, with the possibility of a remote check of the operator in case of malfunctions.



*Fig. 5.20.- The 3D representation of the SPES horizontal handling device. The machine is able to move the target chamber from the lead box to the FE and vice versa. This part of the device will be place over the AGV.*

After the target chamber is placed, the machine will leave the radiation area and the target camera will be connected to the beam pipes, ready for the irradiation stage. A similar procedure is followed in order to remove the target chamber after the irradiation process.

## **B) The vertical handling system**

The second device that was studied was the vertical one. The machine is located in a room just above the irradiation room on the SPES building. This device consists of a rigid frame that moves in a special rail, in which it is inserted a dedicated actuator device in order to guarantee a precise connection with the target chamber, as represented in figure 5.22.. These tools have been designed in order to maintaining an extremely high repeatability level during the insertion and extraction process.

The system performs a series of sequential operations: initially the lead box is positioned by operators with the aid of a motorized lift above the frame of the machine; then the vertical device leaves the loading point and, after removal of the caps on the roof of the irradiation room roof, goes towards the center of the bunker access hole in which the chamber must be replaced.

Once arrived at the working point, the machine lifts the target chamber from the lead box, and starts the descent towards the irradiation bunker; after placing the target chamber on the FE coupling table the machine disconnects itself from target chamber, returns to the upper floor and

closes again the room roof and returns to the loading position where a user can download the lead box and place it in a special depository.

In the planar motion table is placed a suitable tool dedicated to engaging with the target chamber. The whole device has a size of about 1.5m<sup>3</sup>. The first step will be removing the 'cap' in concrete, using the crane. You can then pick up the car by crane and go vertical in the hole. The machine will be lowered by crane and will be inserted and supported in a slit between the irradiation room and shed.

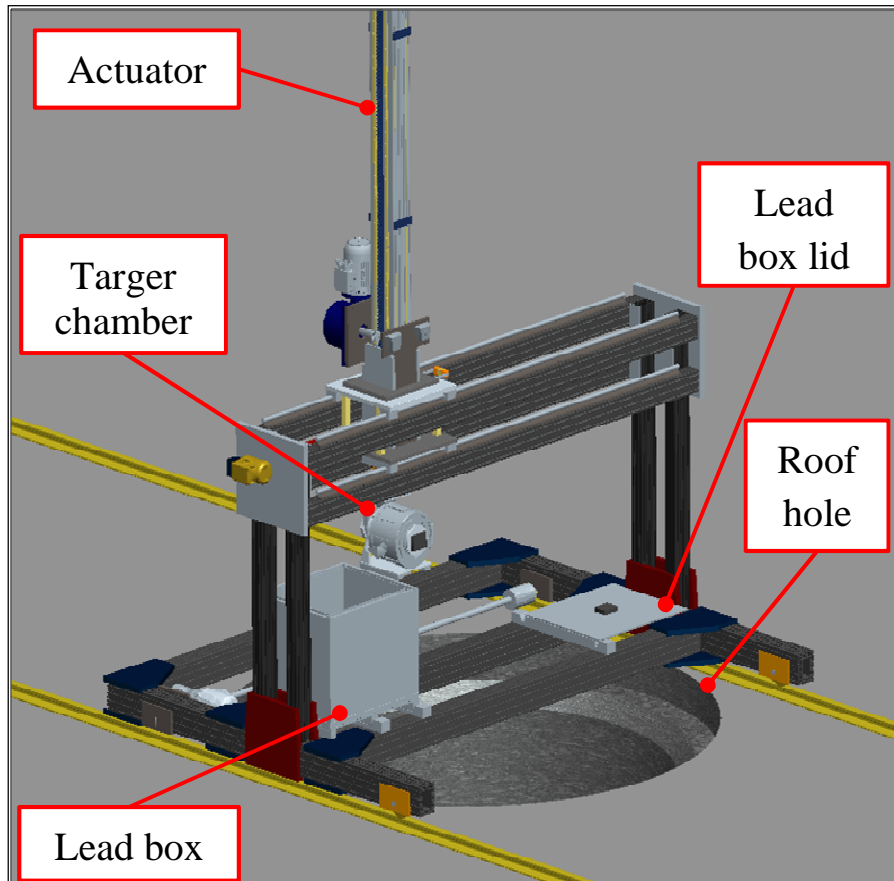


*Fig. 5. 22: The 3D representation of the SPES vertical handling device. The machine is positioned over the roof hole just above the irradiation room.*

Once positioned and centered in the frame, the hydraulic cylinder rods, which guarantees a retracted length of 2 meters and a capacity of 1000N, can be relaxed allowing the attachment of the machine room with the target placed in the front end below.

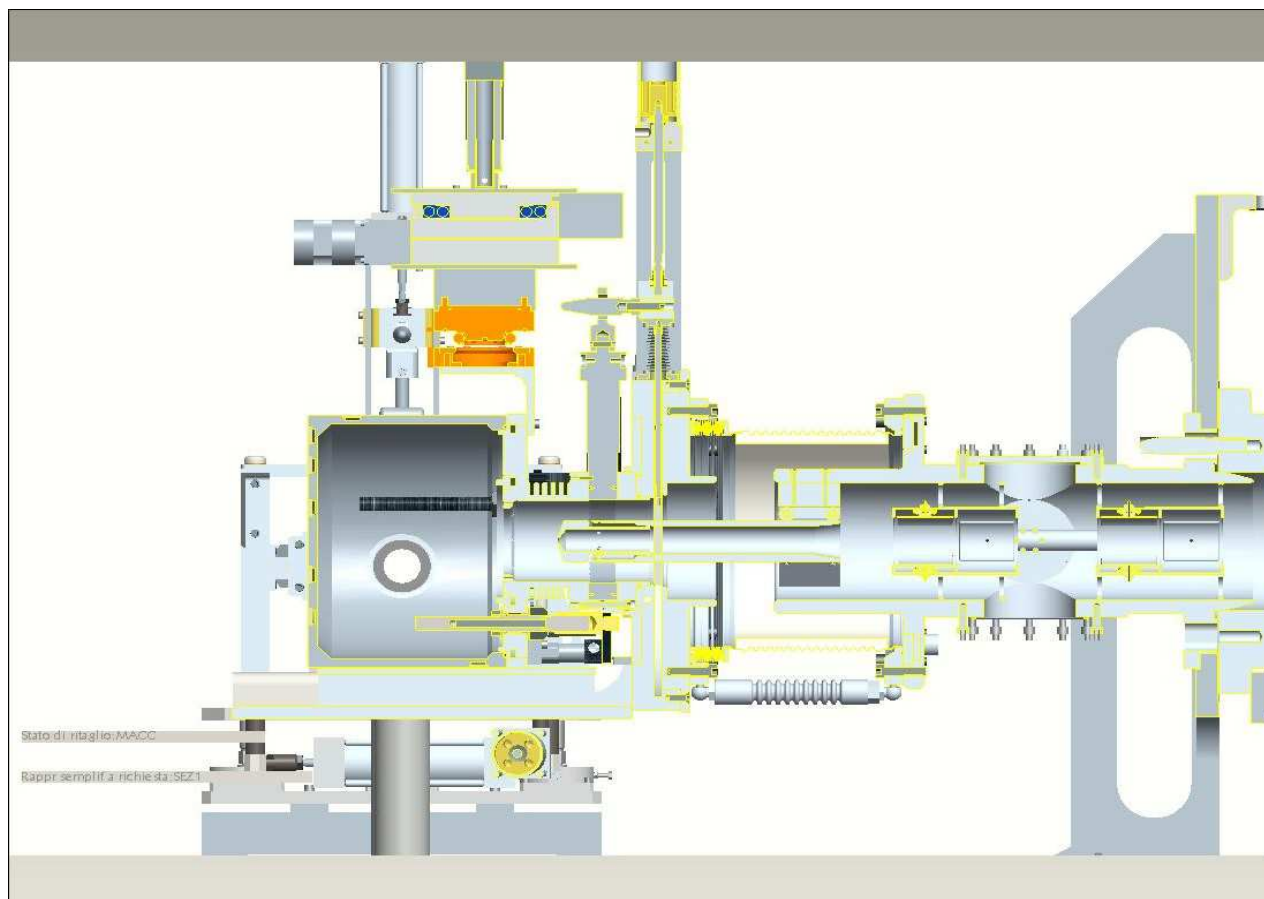


*Fig. 5. 23: The device connected to the target chamber.*

## 5.9 The target prototype

In order to develop the final SPES multi-foil target a research program has been activated to test the target configuration with proton beams of suitable energy. The elective facility to perform these tests is HRIBF (Holified Radioactive Ion Beam Facility) at ORNL [23]. HRIBF is an ISOL RIB facility based on a primary beam of protons at 40 MeV of energy and with current intensity up to 20  $\mu\text{A}$ . Two different tests have been performed in the last years with the target prototype, which has dimensions scaled to 1:5 in comparison to the full scale SPES target. The SPES target prototype consists basically on a graphite tube containing 7 discs with diameters of 13 mm (about 1 mm thick) and a graphite dumper as reported in figure 5.44.

This prototype can be positioned inside the HRIBF target holder, allowing to test in this facility the main ion release characteristics and the capability of the target architecture to dissipate the nominal power density of approximately 600 W/g.

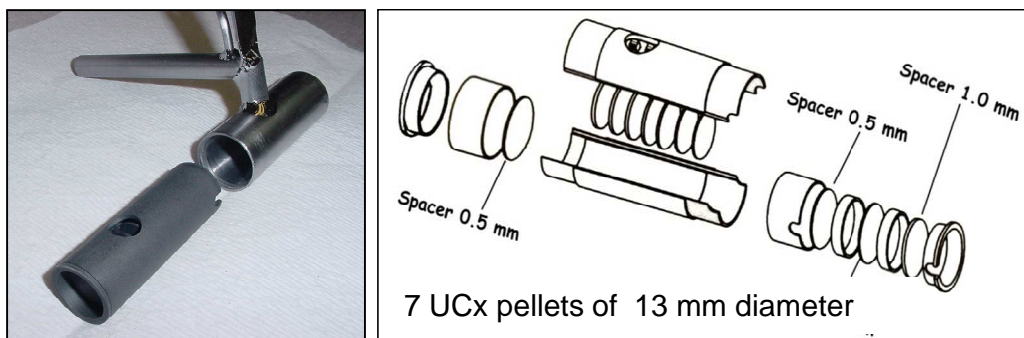


**Figure 5.44:** The SPES target prototype tested at HRIBF.

This scaled version is demonstrated to be fully operative and functional; by means of a scale factor the data collected in this work can be used to predict the behavior of the real scale target once installed in the SPES facility. The first experiment was performed in 2007 using SiC target discs, whereas the second was carried out in 2010 using UC<sub>x</sub> discs of 4 g/cm<sup>3</sup> density each. All isotopes produced in the target were ionized thanks to the Electron Beam Plasma Ion Source (EBPIS).

#### 5.9.1 On-line test of the SiC target prototype

The use of SiC disks is devoted to the production of exotic aluminium beams, <sup>25</sup>Al and <sup>26</sup>Al, which are isotopes of astrophysical interest both at HRIBF and EXCYT. The temperature data of the first test performed in 2007 with SiC disks confirm the prediction [24] of thermal simulations.

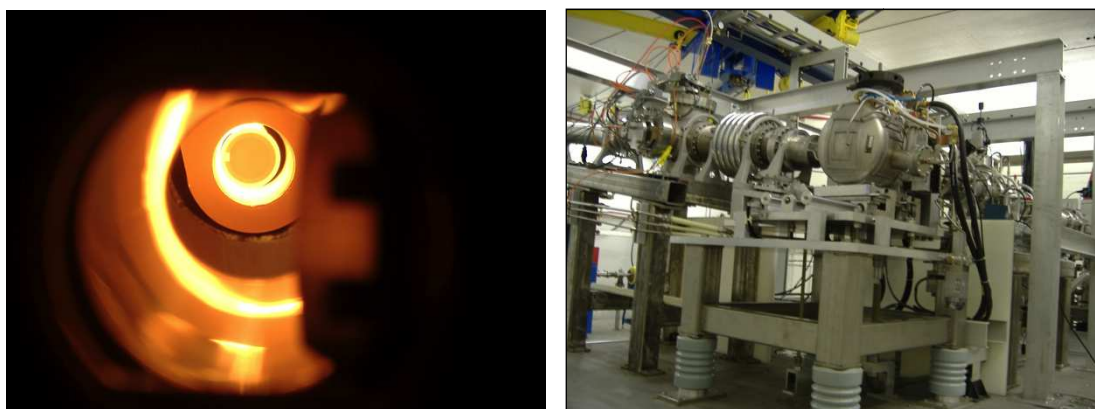


**Figure 5.45:** SiC SPES target inside the target heater (left) and the target area at HRIBF (right).

A comparison between different target configurations and materials will be done. The aluminium isotopes production was measured as a function of proton current and heater temperature. The results are reported in figure 5.46.

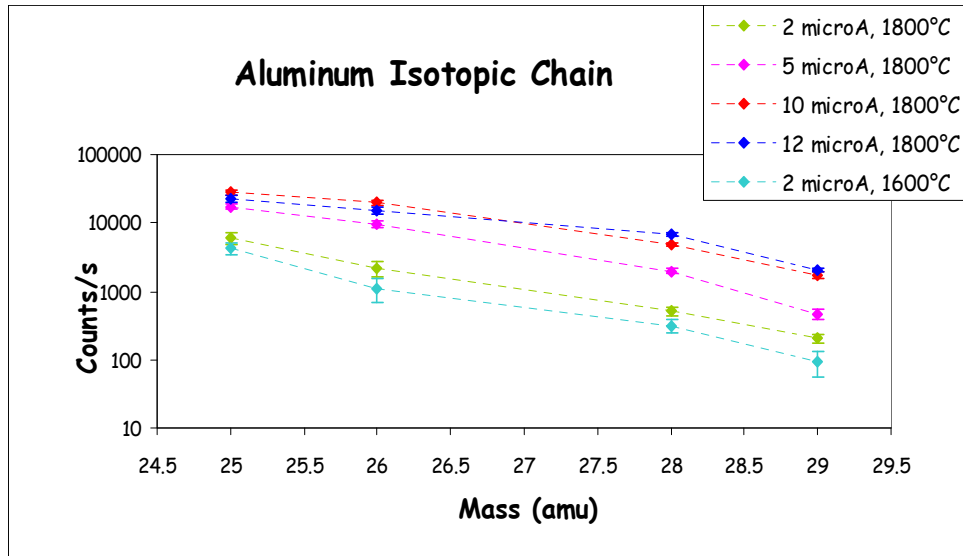


Figure 5.46: Aluminium isotopes production of SiC SPES target at HRIBF.

The target performance was considered very satisfying and this target is actually used at HRIBF.

#### 5.9.2 On-line test of the $UC_x$ target prototype

The SPES  $UC_x$  target prototype was tested on line at HRIBF using a 40 MeV proton beam, coming from the Tandem, with intensity values of approximately 50 nA. The procedure for this experimental test was to span a total number of 36 masses ranging from 72 to 141, measuring yields current amount (by means of the Faraday cup) and saving the gamma-decay spectra. Calculation of the yield of different isotopes, as reported in figure 5.47, was carried out analyzing the gamma-ray spectra obtained by coupling the Ge detector with a multi-channel analyzer (MCA).

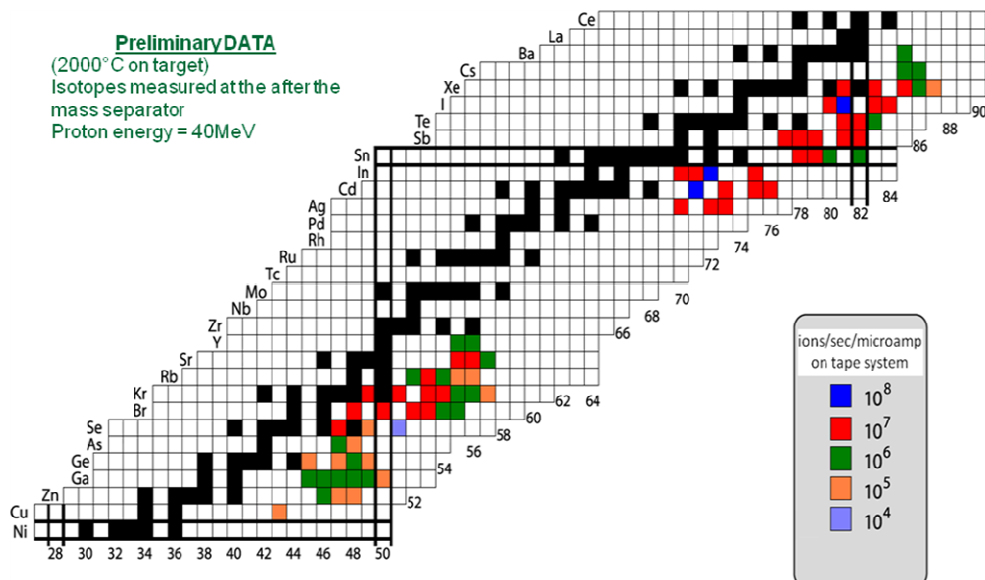
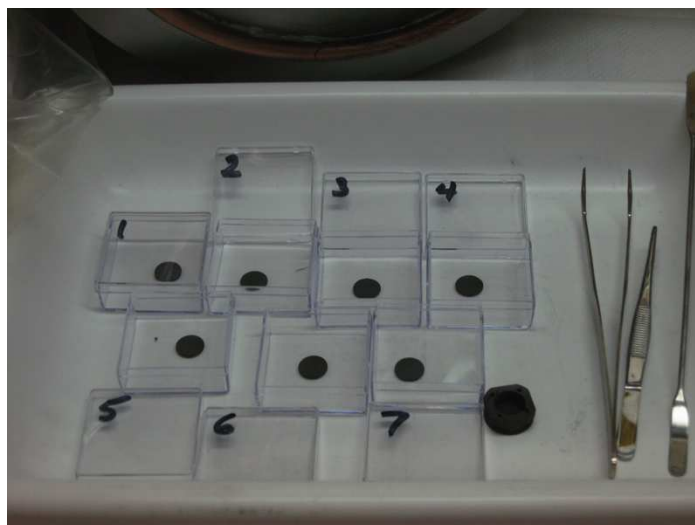


Figure 5.47: The preliminary result of the neutron-rich isotopes collected.

After data collection, following a week of cooling down time, a visual inspection on the uranium carbide disks used during the experiment was done, and no significant structural changes or breakdown were observed (see figure 5.48).



**Figure 5.48:** Seven discs after on-line tests

### References

- [1] A. Andrichetto, Proceeding of Exon 2004 Internatioal Conference (2004).
- [2] P.C. Stevenson et al., Phys. Rev. **111** (3), 886 (1958).
- [3] S. Baba et al., Nucl. Phys. A **175**, 177 (1971).
- [4] B.L. Tracy et al., Phys. Rev. C **5** (1), 222 (1972).
- [4a] M. Re et al. RNB7 conference proceedings, Cortina, Italy, July 2006, in publication
- [6] A. Andrichetto, S. Cevolani, C. Petrovich, Eur. Phys. J. A **25**, 41 (2005).
- [7] A. Andrichetto, C. Antonucci, S. Cevolani, C. Petrovich, M. Santana Leitner, Eur. Phys. J. A **30**, 591 (2006).
- [8] Denise B. Pelowitz (Editor), MCNPX™ User's manual, Version 2.5.0, LA-CP-05-0369 (2005).
- [9] H.W. Bertini, Phys. Rev. **131** **4**, 1801 (1963).
- [10] A. Andrichetto, C.M. Antonucci, S. Cevolani, C. Petrovich, ENEA contribution to the design of the thin target for the SPES project, FIS-P815-020 (ENEA, 2006), <http://www.bologna.enea.it/publicazioni.html>.
- [11] Timoshenko, Goodier, Theory of Elasticity (McGraw Hill, 1970).
- [12] Z. Zudans, T.C. Yen, W.H. Steigelmann, Thermal Stress Techniques in the Nuclear Industry (Elsevier, 1965).
- [13] H.J. Matzke, Science of advanced LMFBR fuels (North Holland, 1980).
- [14] S. Agostinelli et al., Nucl. Instr. Meth. A **506**, 250 (2003).
- [15] M. Santana Leitner, A Monte Carlo Code to Optimize the Production of Radioactive Ion Beams by the ISOL Technique, PhD. Thesis, UPC-ETSEIB / CERN (2005).
- [16] J. Crank, The Mathematics of Diffusion, Clarendon Press (1956).
- [17] R. Kirchner, Nucl. Instr. Meth. B **126**, 135–140 (1997).
- [18] Y. Zhang et al., Nucl. Instr. and Meth. in Phys. Res. A, **521**, 72–107 (2004).
- [19] G. D. Alton, Applied Radiation and Isotopes, **64**, 1574–1603 (2006)
- [20] C. Lau et al., Nucl. Instr. Meth. in Phys. Res. B, **204**, 246-250 (2003)
- [21] D.W. Stracener et al., Nucl. Instr. Meth. in Phys. Res. A, **521**, 126–135 (2004)
- [22] S. Sundell and H. Ravn, NIM B **70** 160 (1992).
- [23] G.D. Alton, NIM A **382** 207 (1996).
- [24] S.Cevolani FIS-P815-022